Imperial College London
Department of Physics

Simulating Plasma Wakefield Acceleration

James Alex Holloway

September 2010

Supervised by Dr Zulfikar Najmudin

Submitted in part fulfilment of the requirements for the degree of Master of Science in Quantum Fields and Fundamental Forces of Imperial College London

Abstract

A theoretical model of a 1D Gaussian density profile beam driving plasma wakefield acceleration is derived and the optimum beam length for resonant excitation of the wakefield is found to be $\sigma = \sqrt{2}/\kappa_p$. Then the particle-in-cell code OSIRIS is used to simulate this plasma-beam interaction for a range of beam densities and beam lengths, and the amplitude of the resulting wakefield is found to closely agree with the predictions of the model. Finally A 2D cylindrical simulation of the untreated Super Proton Synchrotron beam is examined and found to be unsuitable to drive plasma wakefield acceleration.

Contents

1 Introduction **8**

1.1 Conventional Radio Frequency Accelerators 8

1.2 Principles of Plasma Accelerators 9

1.3 Plasma Wakefield Accelerators 10

1.4 Electron Injection Techniques 11

2 Theory **13**

2.1 The Plasma Frequency 13

2.2 1D Linear Model 14

2.3 Non-linear Waves 21

2.4 Efficiency 23

2.5 Self modulation of long proton beams 23

3 Data Analysis and Discussion **25**

3.1 1D Simulations In OSIRIS 25

3.1.1 A Typical 1D Simulation 25

3.1.2 Maintaining Pseudo 1D Symmetry 27

3.1.3 OSIRIS Anomaly 28

3.1.4 Low Density Beam Length Parameter Scans 30

3.1.5 High Density Beam Length parameter Scans and Non-linear frequency shift 33

3.2 2D-Simulations 36

4 Conclusions **42**

5 Appendix **45**

.1 Institutes with Interest in using the SPS Beam for PWA 45

.2 Template Input Deck for 1D Parameter Scans 45

List of Figures

1.1 Illustration of a beam inducing a plasma wakefield 11

2.1 1D analytic model (2.23) of the plasma response to a Gaussian proton beam with $\sigma = 0.0011(c/\omega_p)$ and $n_b/n_e = 0.001$ 17
2.2 1D analytic model (2.23) of the plasma response to varying lengths of a fixed charge Gaussian proton beams with $\sigma = 0.0011(c/\omega_p)$ and $n_b/n_e = 0.001$ 17
2.3 1D model of plasma response to varying lengths of a non-fixed charge proton beam 19
2.4 wakefield amplitude as function of beam length, characterised by σ, for the truncated Gaussian model (blue) and the true Gaussian model (red) 20
2.5 Difference in wakefield amplitude profiles between truncated and non truncated models 2.26 2.32 as function of beam length . 21

3.1 1D OSIRIS simulation of plasma electron response (blue) to a proton driving beam (red) where $\sigma = (13\pi/40) * (c/\omega_p)$ and the number density of the beam is $n_{b\ peak} = n_e/1000$ 25
3.2 Plasma's electron and ion response to proton driver beam . . . 26
3.3 Three data dumps three simulations, at the same time step, that only differ by resolution. The top, middle and bottom plots have resolution of 2.5, 10 and 15 respectively 27
3.4 Re-plot of figure 3.1. A 1D OSIRIS simulation of plasma electron response (blue) to a proton driving beam (red) where $\sigma = (13\pi/40) * (c/\omega_p)$ and the number density of the beam is $n_{b\ peak} = n_e/1000$ 28
3.5 Proton beam that excited the plasma in figure 3.4 at different time steps 29
3.6 The resulting plasma electron wakefield at two different time steps 29
3.7 The resulting plasma ion wakefield at two different time steps . 30

3.8 Three beams of density $n_{b_{max}} = 0.003 \times n_e$ truncated at $\sigma = 1, 2, 3$ for red, green, blue respectively 32
3.9 Amplitude of lesser resonant peaks vs Fractional beam density at hard-edged truncation 32
3.10 The amplitude of wakefield oscillation as a function of σ for 1D simulations (Batch C 3.2) of Gaussian density profile beams of peak number density $n_b = n_e/1000$ (red) and for the variable charge truncated Gaussian beam model (blue) 2.32 34
3.11 Data dump of $n_b/n_p = 1$ 1D simulation at resonance ($\sigma = 8\pi/40$) showing saw-tooth electron plasma density profile . . . 34
3.12 Wakefield Amplitude plotted against beam length, σ, for high density batches G, H, I. Absolute measurement of wakefield amplitude. 35
3.13 Parameter Sets for 2D cylindrical SPS beam simulations 36
3.14 The SPS beam profile described by equation 3.2 and set 3 parameters from table 3.13. The axis spanning 0 to 6000 is increasing in the direction of propagation and one unit is $1/(5 \times \kappa_p)$ meters. The axis spanning 0-20 is in the radial direction, where the centre of the beam sits at r = 0 and one unit is $1/(5 \times \kappa_p)$ meters. The axis spanning 0-1.6 $\times 10^{-3}$ is the proton charge number density 37
3.15 The difference between the SPS beam at $t = 0$ as seen in figure 3.14 and the final beam at $t = 144 \times 10^{-9} s$ The axis spanning 0 to 6000 is increasing in the direction of propagation where one unit is $1/(5 \times \kappa_p)$ meters. The axis spanning 0-25 is in the radial direction, where the centre of the beam sits at r = 12 and one unit is $1/(5 \times \kappa_p)$ meters. The axis spanning -1 to 1 is the proton charge number density 38
3.16 The plasmas' response to the Gaussian beam seen in figure 3.14. The axis spanning 0 to 6000 is increasing in the direction of propagation where one unit is $1/(5 \times \kappa_p)$ meters. The axis spanning 0-25 is in the radial direction, where the centre of the beam sits at r = 12 and one unit is $1/(5 \times \kappa_p)$ meters. The axis spanning $0 - 3$ is the proton charge number density 39

3.17 The Top left plot shows the first 100 cells of high amplitude oscillation, as seen in figure 3.16. The top right plot then shows wake siting at $z = 30$. The bottom plot shows the amplitude of oscillation along the axis of propagation. The axis spanning 0 to 100 is increasing in the direction of propagation where one unit is $1/(5 \times \kappa_p)$ meters. The axis spanning 0-1 is in the radial direction, where the centre of the beam sits at r = 2.5 and one unit is $1/(5 \times \kappa_p)$ meters. The axis spanning 0-1.6 $\times 10^{-3}$ is the proton charge number density 40
3.18 This is a crop between 2600 to 3000 of the 6000 data points along the axis of propagation and shows a low amplitude wakefield. Each 'step' corresponds to a fractional density change of $(\Delta n_e/n_e = 0.0000004)$. 41

List of Tables

3.1 1D-Simulation Parameters 31
3.2 Parameter scans over σ for low density gaussian proton beams . 31

1 Introduction

This chapter is an introduction to particle beam driven plasma wakefield accelerators. The first section compares conventional radio frequency particle accelerators with plasma wakefield accelerators. Then oscillations and electric field strengths in plasmas are discussed and finally the limitations of proton driven plasma wakefield acceleration (PD-PWA) are examined.

1.1 Conventional Radio Frequency Accelerators

Since the 1930's, particle accelerators have been used to further understand the fundamentals of particle physics. Colliders at the energy frontier are able to test the predictions of the standard model, and by proving or disproving them they advance the field of particle physics. Modern day accelerators are no longer just used for fundamental research, but have a wide range of applications in industry, pharmacology and radiotherapy. New discoveries come as particle accelerators are able to reach higher energy regimes, but as the energies increase so does the size and cost of the accelerators.

Constructing and running modern high energy particle accelerators is an expensive and demanding task. Large facilities such as CERN, SLAC and Tevatron have particle accelerators many that are kilometres long. These modern particle accelerators consist of a metal cavity wherein particles are accelerated using an alternating electric field. Electric field gradients greater than $100 MV m^{-1}$ ionise the metal itself, destroying the accelerator, so to reach higher particle energies one has to increase the length over which the particles are accelerated. With a circumference of 27km CERN is already the largest machine in the world, and with a budget of 6.19 Billion as of 2010 it is one of the most expensive scientific instruments ever built [1]. To keep ever increasing the length of accelerators is not an economically viable option. Plasmas offer a solution to this problem as they can support far greater electric fields and therefore achieve the same energy gains over much shorter distances and, being already ionised, are resistant to further destruction. For these reasons plasma accelerators are an attractive alternative to conventional accelerators.

1.2 Principles of Plasma Accelerators

A plasma can be defined as a quasi neutral gas of charged and neutral particles which exhibit collective behaviour [2]. A key quantity that characterises a plasma is the plasma frequency 1.1. Consider displacing electrons in a cold plasma. An electric field is produced that acts as a restoring force. The electrons accelerate back towards the region of unmoved ions, gaining kinetic energy. Having reached their original equilibrium position, they overshoot, due to the kinetic energy gained from the electric field, and an oscillation is set up. This is called a Langmuir oscillation [3] and the frequency of this oscillation is the plasma frequency. The ions' inertia are too large to respond to the short period of the oscillation and are considered static.

$$\omega_p = \left(\frac{e^2 n_e}{m_e \epsilon_0} \right)^{1/2} \tag{1.1}$$

Here, e is the electron charge, m_e is the electron mass, ϵ_0 is the permittivity of free space and n_e is the electron plasma number density. Another important quantity when considering PWA is the plasma wavelength.

$$\lambda_p = \frac{2\pi c}{\omega_p} \tag{1.2}$$

The optimum low density beam length for resonant excitation of a wakefield is $L_b = \lambda_p/2$ for constant density hard-edged beams and the standard deviation is $\sigma = \pi/2\kappa_p$[4] for Gaussian density profile beams. Consider the 1D case. The first half of the beam will exert a pulling force on the plasma electrons. At the point at which those electrons have reached their maximum oscillation amplitude, $\lambda/4$, the beam will be centred on them and exert no net force. Then on the electrons' return journey the sign of the force of the beam will change, and the pushing force will reinforce the oscillation setup by the first half of the beam. The magnitude of the electric field that these electron plasma waves are able to support is given by 1.3, which corresponds to a density change of $\Delta n_e/n_e = 1$, beyond which they succumb to wave breaking. For high density driving beams where beam number density,n_b, is approximately equal to the plasma number density, n_p, the electrons begin to move relativistically and the plasma response becomes non-linear.

$$E = \frac{\omega_p m_e c}{e} \tag{1.3}$$

The resonance condition effectively limits the attainable electric field strength, and therefore acceleration of the witness beam. This is because high electric

field strengths require high density plasmas 1.3, which need short beams to resonantly excite them. For a plasma density of $n_p = 10^{21}/m^3$ simulations indicate energy gains can exceed $200MeV/m$ [5], but this requires high density beams of length $L_b = 5.78 \times 10^{-4}$, a technically challenging task.

The Super Proton Synchrotron beam at CERN has a rms bunch length of 0.12m [**?**], which is over a hundred times longer than the plasma wavelength at this density. This would resonantly excite a plasma of $n_p = 1.93 \times 10^{16}$, which can support a maximum electric field strength of 1.33×10^{16}, over 200 times weaker than the field strength at $n_p = 10^{21}/m^3$, and would require an accelerator length of 70km in order to accelerate electrons to $1TeV$. Naively then it would seem the SPS beam is unsuitable for PD-PWA. G. Xia et al. consider using a 400m long bunch compressor on the SPS beam in order to achieve the desired beam length [**?**]. However, there is a self modulation instability that affects beams of length $L_b > \lambda_p$, modulating them at the plasma frequency. This results in longer beams being cut into a series of short pulses, each of which has $L_b \sim \lambda_p$, that reinforce the wakefield established by the pulse in-front, the cumulative effect being a high amplitude wakefield. One of the focuses of this dissertation is to use the Particle-in-Cell code OSIRIS to simulate the untreated SPS beam and investigate its suitability for PWA at high densities.

1.3 Plasma Wakefield Accelerators

A plasma wakefield accelerator is a device that fires a driving beam into a plasma and uses the resulting oscillation of plasma electrons to accelerate a witness beam. The process works by creating an accelerating structure that co-moves with the beam. Following the beam are alternating regions of high and low electron density that have a transverse focusing electric field and a longitudinal accelerating electric field. Consider a short relativistic proton pulse driving a plasma. The beam enters the plasma and attracts the plasma electrons towards the axis of beam propagation, leaving the heavier ions behind. The electrons gain kinetic energy as they accelerate towards the beam and overshoot the axis, leaving a positively charged region of ions behind the beam. A Langmuir oscillation is set up and as the electrons rush back in to fill the positively charged region they 'pinch' together behind the propagating proton beam, creating a strong longitudinal electric field. A schematic illustration of plasma wakefield acceleration is shown in figure 1.1.

This accelerating 'bubble' structure co-moves with the driving proton beam and can extend several λ_p behind the beam [6, 7] before heating effects dom-

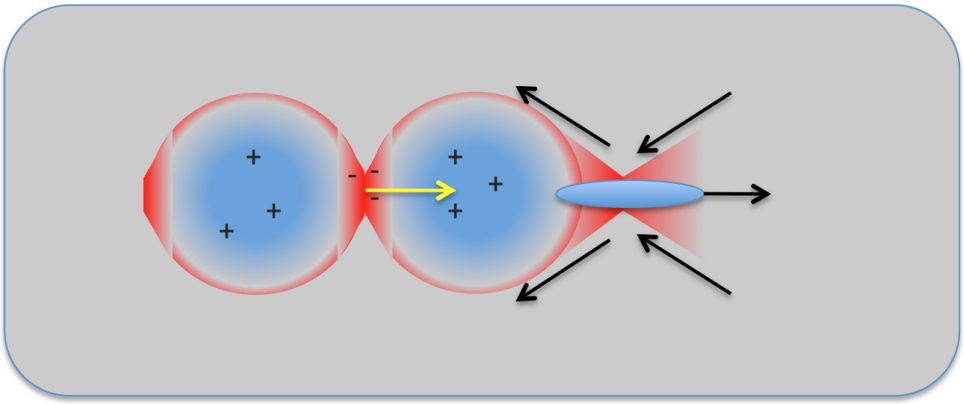

Figure 1.1: Illustration of a beam inducing a plasma wakefield

inate. Any electrons injected into the rear of this structure will be accelerated by the longitudinal electric field. The resulting 'plasma wakefield acceleration' has been experimentally shown to give accelerating gradients of order GeV/cm [8, 9], far greater than conventional radio frequency (RF) accelerators. Both relativistic beams of charged particles [10] and intense laser pulses [11, 12] have successfully been used to accelerate electron witness beams to high energies. It is crucial for the phase velocity of the driving beam to be close to the speed of light, c, so that the accelerated electrons do not outrun the driving beam and escape the accelerating structure.

1.4 Electron Injection Techniques

It is necessary that fast electrons are present in an established wakefield for them to remain in the accelerating structure long enough to gain significant energy. Wave-breaking can provide these fast electrons [13], but that requires a high density driving beam ($n_b \sim n_p$). In the low density regime there are alternative techniques to create fast electrons that will briefly be discussed here. An electron beam with energy on the order of MeV can be fired directly along the axis of propagation, and if timed and aligned perfectly, the electrons will be caught in the accelerating structure and taken to higher energies [14]. Alternatively, if an electron driver is used that has a length comparable to that of the plasma wavelength, the rear of the beam can be accelerated by the wakefield [15]. Another technique is to dope a neutral gas with heavier elements. This technique relies on the driving beam to ionise the gas and create the plasma itself. As it does so a wakefield is set up, but the heavier elements hold onto their electrons under stronger external electric fields than the background gas.

Once the electric field provided by the driving beam approaches the magnitude of the electric field binding the inner electrons to their host atoms, barrier suppression ionisation occurs. The point at which the electric field strength of the beam is approximately equal to the electric field strength that binds the electron to the nucleus the heavy atom is within the established wakefield - as other atoms with lower binding energies have long been ionised. These newly ionised electrons can then catch the wakefield and be accelerated.

In the following chapters important concepts to PWA are introduced and a 1D model for the excitation of a plasma by a gaussian density profile beam is derived and the resonant beam length found. Then 1D OSIRIS simulations are explored and compared to the predictions of the model. Finally a simulation of the SPS beam is analysed and its feasibility in driving PWA discussed.

2 Theory

This section outlines the theoretical concepts relevant to proton-plasma interactions. First, the resonance conditions for proton-driven plasma wakefield acceleration is discussed. Then a linear 1D model of proton-driven plasma wakefield interaction is derived. Both the concepts and the model apply to the PIC simulations in the Data Analysis section.

2.1 The Plasma Frequency

Starting off this chapter is the simple derivation of the plasma frequency quoted in the introduction 1.1. Assuming the same set up of the displacement of a sheet of electrons in a cold plasma in section 'Principles of Plasma Accelerators' and starting with the linearised continuity equation, equation of motion and gauss' law:

$$\nabla.\mathbf{E} = -\frac{e\Delta n_e}{\epsilon_0} \tag{2.1}$$

$$-e\mathbf{E} = m_e\frac{\partial^2\mathbf{x}}{\partial t^2} \tag{2.2}$$

$$\frac{\partial\Delta n_e}{\partial t} + n_e\nabla.\mathbf{v} = 0 \tag{2.3}$$

Where $\mathbf{E}$ is the electric field, $\mathbf{x}$ is the spacial direction and $\mathbf{v}$ is the velocity. Assuming all oscillations are one dimensional and sinusoidal in space and time, and writing quantities in terms of an equilibrium term and an oscillating term, we find $n = n_e + \Delta n_e$, $\mathbf{E} = \mathbf{E}_0 + \mathbf{E}_1$, $\mathbf{v} = \mathbf{v}_0 + \mathbf{v}_1$ and:

$$\Delta n_e = \Delta n_e e^{i(\kappa x - \omega t)} \tag{2.4}$$

$$\mathbf{E} = \mathbf{E}_1 e^{i(\kappa x - \omega t)} \tag{2.5}$$

$$\mathbf{v} = \mathbf{v}_1 e^{i(\kappa x - \omega t)} \tag{2.6}$$

Substituting 2.5 into 2.1, 2.4 and 2.6 into 2.3 and 2.6 into 2.2 we find:

$$im_e\omega v = -eE \tag{2.7}$$

$$\omega\Delta n_e - \kappa n_e v = 0 \tag{2.8}$$

$$i\kappa E = e\Delta n_e/\epsilon_0 \tag{2.9}$$

Where κ is the wavenumber of the plasma. Solving equations 2.7, 2.8, 2.9 for ω and eliminating E, κ, Δn_e and v, we find an expression for the plasma frequency ω_p:

$$\omega_p = \left(\frac{e^2 n_e}{m_e \epsilon_0}\right)^{1/2} \tag{2.10}$$

2.2 1D Linear Model

1D solutions can be usefully applied. For example, a strong magnetic field can constrict the movement of charged particles to the field lines and reduce the system to 1D. To analyses the density profile of a plasma perturbed by a charged driving beam traveling close to c, consider the plasma in three regions. Region A is the plasma ahead of the driving beam. It remains unperturbed because the beam is traveling close to c, and fields will not propagate faster than it. Region B is the plasma being perturbed by the beam as it passes. Region C is the perturbed plasma behind the beam. Region A is trivial, B is described by 2.11 with a forcing term, and C is described by 2.12 with the amplitude of density oscillation determined by region B. This derivation focuses on Region B and then uses boundary conditions to find region C.

In the linear regime the electrons oscillations can be described by simple harmonic motion. We start with Newton's second law 2.11:

$$\frac{d^2\alpha}{dt^2} m_e + \frac{n_e e^2}{\epsilon_0}\alpha = 0 \tag{2.11}$$

Dividing through by m_e puts 2.11 in terms of ω_p, refequ:plasmafreq:

$$\frac{d^2\alpha}{dt^2} + \omega_p^2\alpha = 0 \tag{2.12}$$

The driving force on an electron in the plasma from the beam is calculated. Assume a Gaussian density profile for a proton beam, we find its Electric field

using Gauss's law:

$$\nabla.E_b = \frac{\rho_b}{\epsilon_0} = \frac{e}{\epsilon_0} n_{b_{(x)}} = \frac{e}{\epsilon_0} \frac{n_{b_0}}{\sqrt{2\pi\sigma^2}} e^{\frac{-(x-ct)^2}{2\sigma^2}} \tag{2.13}$$

It is crucial to note at this point that the Gaussian chosen for the beam profile has a total area of 1 - normalised by the co-efficient $\frac{1}{\sqrt{2\pi\sigma^2}}$. So the total charge of the beam, n_{b_0}, remains constant. Therefore as the beam length increases, the beam is 'stretched' and the charge density decreases. Later we will consider the case where the total charge of the beam is not fixed, and is instead a function of the beam length. Integrating 2.13:

$$E_b = \frac{e n_{b_0}}{\epsilon_0 2} erf\left(\frac{x-ct}{\sqrt{2}\sigma}\right) \tag{2.14}$$

So the force acting on a plasma electron is found to be:

$$F = -eE_b = \frac{-e^2 n_{b_0}}{\epsilon_0 2} erf\left(\frac{x-ct}{\sqrt{2}\sigma}\right) \tag{2.15}$$

Including 2.15 as the forcing term in 2.11 the forced oscillation in region B is found 2.16

$$\frac{d^2\alpha}{dt^2} + \omega_p^2 \alpha = \frac{-e^2}{\epsilon_0 m_e} \frac{n_{b_0}}{2} erf\left(\frac{x-ct}{\sqrt{2}\sigma}\right) \tag{2.16}$$

Expressing this in terms of the density change of the plasma electrons, Δn_e, we find:

$$\frac{d^2\Delta n_e}{dt^2} + \omega_p^2 \Delta n_e = \omega_p^2 \frac{n_{b_0}}{\sigma\sqrt{2\pi}} e^{\frac{-(x-ct)^2}{2\sigma^2}} \tag{2.17}$$

Transforming to the Quasi-Static frame, co-moving with the beam [16]. We define $\xi = x - ct$ and find:

$$\frac{d}{dt} = \frac{\xi}{dt}\frac{d}{d\xi} + \frac{d\tau}{dt}\frac{d}{d\tau} = -c\frac{d}{d\xi} + \frac{d}{d\tau} = -c\frac{d}{d\xi} \tag{2.18}$$

$$\frac{d^2\Delta n_e}{d\xi^2} + \frac{\omega_p^2}{c^2}\Delta n_e = \frac{\omega_p^2}{c^2} \frac{n_{b_0}}{\sigma\sqrt{2\pi}} e^{\frac{-\xi^2}{2\sigma^2}} \tag{2.19}$$

We note that the form of this equation is $y'' + \omega y = f_{(\xi)}$. Using Green's functions the solution to this general equation is:

$$y_{(\xi)} = \int_0^\infty G_{(\xi,\xi')} f_{(\xi')} d\xi' = \int_0^\xi \frac{1}{\omega_p} \sin\omega(\xi - \xi') f_{(\xi')} d\xi' \tag{2.20}$$

Where $G_{(\xi,\xi')} = \frac{1}{\omega}\sin(\omega(\xi - \xi'))f_{(\xi')}$ for $0 < \xi' < \xi$ and 0 otherwise. Taking $\omega_p/c = \kappa_p$, where κ_p is the wavenumber of the plasma, and applying the solution to 2.19:

$$\Delta n_{e(\xi)} = \kappa_p \frac{n_{b_0}}{\sigma\sqrt{2\pi}} \int_0^{\xi} \sin\left(\kappa_p(\xi - \xi')\right) e^{\frac{-\xi^2}{2\sigma}} d\xi' \tag{2.21}$$

An important subtlety to note is that the integral 2.21 is from 0 to ξ, where 0 is the point at which the beam begins and ξ is the point at which the beam ends. There are two problems, firstly the Gaussian is centred at 0 in the quasi-static frame, so integrating over these limits effectively ignores the first half of the beam, leaving an infinitely sharp leading edge. Plasmas respond very differently to hard edged beams and the integral as it stands does not represent the Gaussian beam. Secondly a true Gaussian extends to $\pm\infty$, so the integration limits become $\pm\infty$ to encompass the entire beam we find 2.22.

$$\Delta n_{e(\xi)} = \kappa_p \frac{n_{b_0}}{\sigma\sqrt{2\pi}} \int_{-\infty}^{\infty} \sin\left(\kappa_p(\xi - \xi')\right) e^{\frac{-\xi^2}{2\sigma}} d\xi' \tag{2.22}$$

Integrating 2.22 we find the analytic expression for the variation in the electron density of a plasma being perturbed by a relativistic Gaussian proton beam of fixed charge 2.23.

$$\Delta n_{e(\xi)} = \kappa_p n_{b_0} \sin(\kappa_p \xi) e^{-\frac{1}{2}\kappa_p^2\sigma^2} \tag{2.23}$$

Note that this linear solution applies to situations where the charge density of the driving beam is considerably less than the charge density of the plasma electrons. Plotting $\Delta n_e/n_e$ vs ξ we find a well behaved linear response of the plasma 2.1.

The sinusoid in figure 2.1 extends to $\pm\infty$ with constant amplitude. This is a result of the integration limits and describes region B as discussed earlier. There is no region A in front of the beam or region B behind it as the Gaussian is infinite, so figure 2.1 describes the entire system.

Figure 2.2 plots the amplitude of oscillation against σ and shows the optimum σ of a beam for achieving the highest amplitude wakefield. Unsurprisingly, as the beam length increases from the amplitude of oscillation decreases. This is because the beam's charge density decreases with length. Also note the reverse applies, as σ decreases the beam is compressed, raising its peak density above its initial n_{bpeak} and therefore the amplitude of the established wakefield. This advantageous feature is specific to this fixed charge model. Therefore, for a fixed charge Gaussian beam, the largest amplitude wakefield is achieved as $\sigma \to 0$.

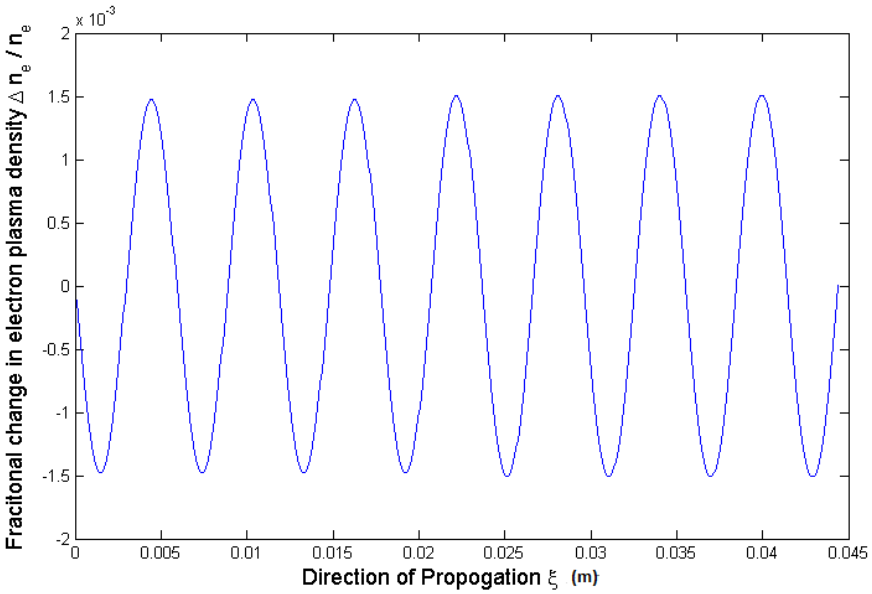

Figure 2.1: 1D analytic model (2.23) of the plasma response to a Gaussian proton beam with $\sigma = 0.0011(c/\omega_p)$ and $n_b/n_e = 0.001$

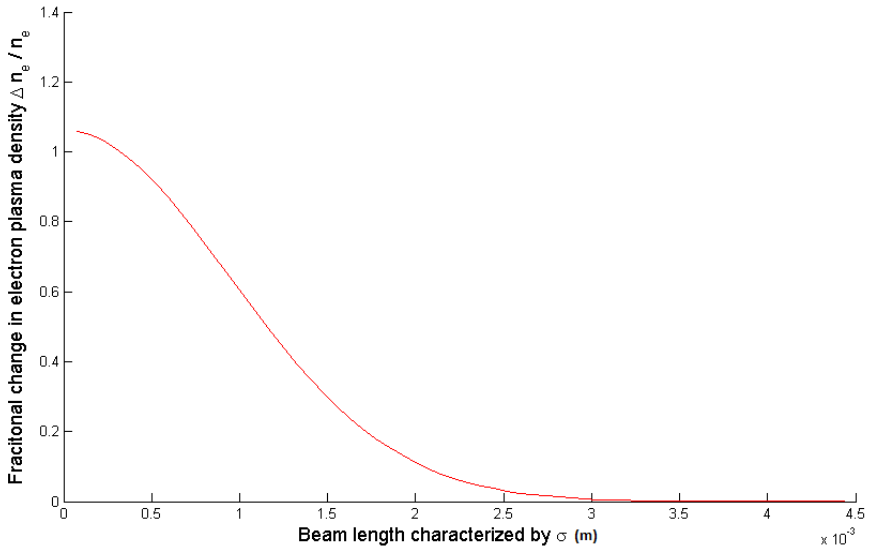

Figure 2.2: 1D analytic model (2.23) of the plasma response to varying lengths of a fixed charge Gaussian proton beams with $\sigma = 0.0011(c/\omega_p)$ and $n_b/n_e = 0.001$

Now we will consider the case where the charge density at the centre of the Gaussian beam profile is fixed, and as the beam length is increased the total charge of the beam increases - the variable charge model. First we modify n_{b_x}

from equation 2.13 by dropping the coefficient that conserved the area of the gaussian:

$$\nabla.E_b = \frac{-en_{b_0}}{\epsilon_0} e^{\frac{-(x-ct)^2}{2\sigma^2}} \tag{2.24}$$

Note the dimension of n_{b_0} is not longer charge, but charge per unit length. Integrating 2.24. Following the same treatment and skipping to the Green's function integral we find 2.25.

$$\Delta n_{e(\xi)} = \sqrt{2\pi}\kappa_p n_{b_0} \int_{-\infty}^{\infty} \sin\left(\kappa_p(\xi - \xi')\right) e^{\frac{-\xi^2}{2\sigma}} d\xi' \tag{2.25}$$

Integrating 2.21 we find the analytical expression for the variation in the electron density of a plasma being perturbed by a variable charge proton beam traveling close to c 2.26.

$$\Delta n_{e(\xi)} = \sqrt{2\pi}\kappa_p n_{b_0} \sigma \sin(\kappa_p \xi) e^{-\frac{1}{2}\kappa_p^2\sigma^2} \tag{2.26}$$

To find the maxima and minima of equation 2.26 we first differentiate and with respect to σ and set it to zero.

$$f(\sigma) = \sigma e^{-\frac{\kappa_p^2\sigma^2}{2}} \tag{2.27}$$

$$f'(\sigma) = (1 - \kappa_p^2\sigma^2) e^{-\frac{\kappa_p^2\sigma^2}{2}} = 0 \tag{2.28}$$

This has two solutions, one at $\sigma = \sqrt{2}/\kappa_p$ and one at $\sigma = \infty$. To find out if they are maxima or minima we differentiate once more and evaluate the function at $\sigma = \sqrt{2}/\kappa_p$ and $\sigma = \infty$

$$f''(\sigma) = (\kappa_p^3\sigma^3 - 3\kappa_p\sigma) e^{-\frac{\kappa_p^2\sigma^2}{2}} \tag{2.29}$$

$f''(\infty) > 0$, and is a minimum, whereas $f''(\sqrt{2}/\kappa_p) < 0$ and is a maximum. Therefore we have found the resonance condition for a variable charge Gaussian profile beam to be:

$$\sigma_{resonance} = \frac{\sqrt{2}}{\kappa_p} \tag{2.30}$$

This important result tells us not only the value of the maximum, but that there is only one maximum for Gaussian profile beams.

Plotting $\Delta n_{e(\xi)}$ against ξ will again show a sinusoidal response of the plasma, however, plotting $\Delta n_{e(\xi)}$ against σ gives us a different result. Figure 2.3 plots

the wakiefield amplitude profile of equation 2.26.

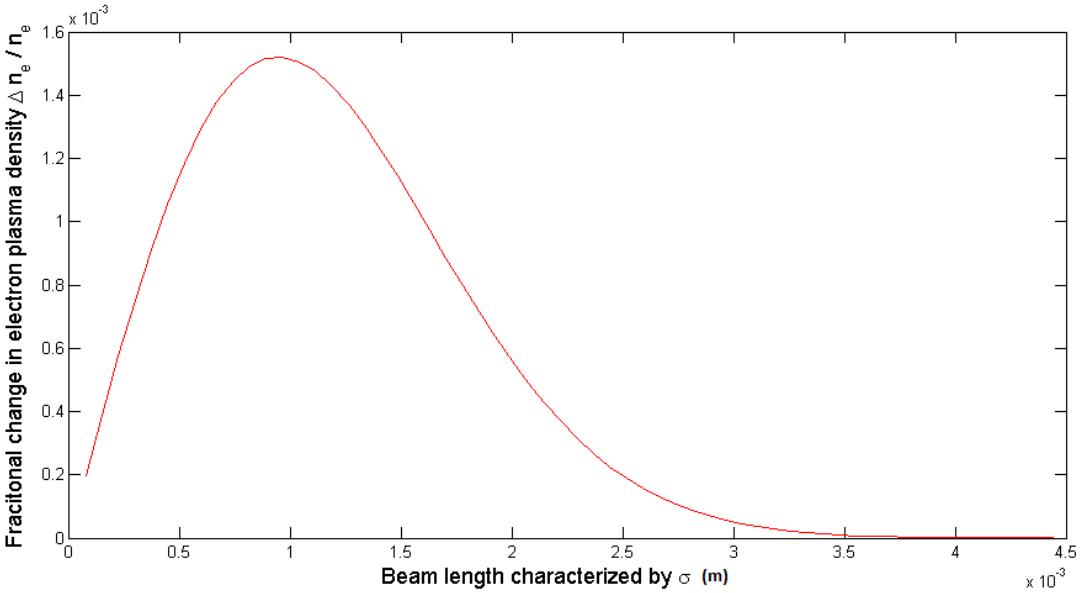

Figure 2.3: 1D model of plasma response to varying lengths of a non-fixed charge proton beam

In this plot $n_{b_0} = n_e/1,000$. Note that as beam length goes to zero so does the amplitude of the resulting wakefield. This makes sense as the charge of the beam is proportional to length in this model, and as the length goes to zero so does the charge of the beam and therefore its effect on the plasma. Using the transformer ratio the maximum energy gain of a witness beam in the wakefield created by a driving beam of resonant beam length is found to be $1.52 \times E_{beam}$. This is assuming that the number of particles in the witness beam is vanishingly small compared to that of the driving beam.

This result, although elegant, is unrealistic. No physical beams are truly infinite and the Gaussian beams simulated in chapter 3 are truncated at $\sigma = \pm 3$ for computational purposes. With this in mind the integration is performed again, with the new integration limits of $\pm 3 \times \sigma$

$$\Delta n_{e(\xi)} = \sqrt{2\pi}\kappa_p n_{b_0}\sigma \int_{-3\sigma}^{3\sigma} \sin\left(\kappa_p(\xi - \xi')\right) e^{\frac{-\xi^2}{2\sigma}} d\xi' \tag{2.31}$$

Integrating 2.31 we find the expression for the variation in the electron density of a plasma being perturbed by a relativistic truncated Gaussian proton beam of variable charge 2.32.

$$\Delta n_e = -\frac{i\sigma}{4}\sqrt{2\pi}e^{-\frac{1}{2}\kappa^2\sigma^2-3i\kappa\sigma-i\kappa x}\left(e^{6i\kappa\sigma}erf\left(\frac{-x+3\sigma+i\kappa\sigma^2}{\sqrt{2}\sigma}\right)+e^{2i\kappa x}erf\left(\frac{x-3\sigma+i\kappa\sigma^2}{\sqrt{2}\sigma}\right)\right)$$
$$+\frac{i\sigma}{4}\sqrt{2\pi}e^{-\frac{1}{2}\kappa^2\sigma^2-3i\kappa\sigma-i\kappa x}\left(+e^{6i\kappa\sigma}erf\left(\frac{3}{\sqrt{2}}+\frac{i\sigma\kappa}{\sqrt{2}}\right)+e^{2i\kappa x}erf\left(-\frac{3}{\sqrt{2}}+\frac{i\sigma\kappa}{\sqrt{2}}\right)\right) \tag{2.32}$$

Figure 2.4 shows the wakefield amplitude induced by the truncated Gaussian beam (blue) as a function of σ and that of the non truncated beam (red) 2.26. Figure 2.4 is over a wider range of values for σ and again the density change Δn_e has been scaled to the fractional density change, $\Delta n_e/n_e$. Note that the density no longer falls and stays at zero as σ increases, instead it 'bounces' back up to a low fractional density before falling back down. The initial bounce is of lower amplitude than the following. This bouncing continues as $\sigma \to \infty$, generating lesser peaks, and is a direct result of the truncation.

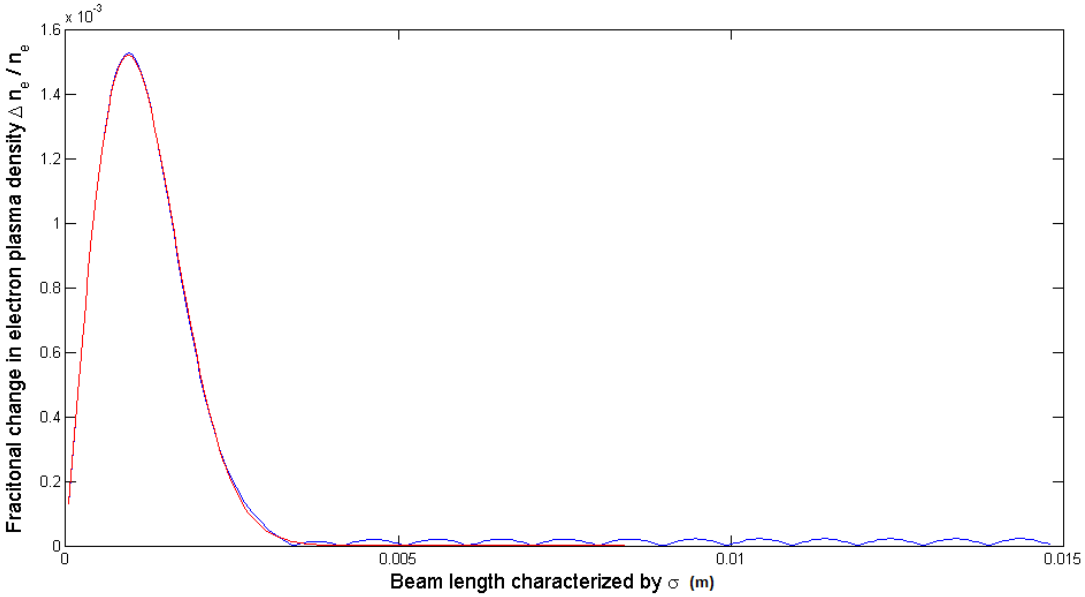

Figure 2.4: wakefield amplitude as function of beam length, characterised by σ, for the truncated Gaussian model (blue) and the true Gaussian model (red)

Figure 2.5 plots the difference between the two wakefield amplitude profiles to investigate the truncations effect. In the region where the Gaussian component of the beam dominates $(\sigma \sim 0 - 0.004)$ the truncations effect both reinforces and diminishes the amplitude of the wakefield. This behaviour changes once the amplitude of oscillation induced by the Gaussian component falls be-

low the amplitude induced by the hard-edge of the truncation ($\sigma \sim 0.004+$). Then the behaviour seen is that of a hard-edged constant density beam, with the amplitude of wakefield oscillation increasing as the length between the two truncations approaches $(\lambda_p/2) \times (2N+1)$ and falling to zero as it approaches $(\lambda_p/2) \times 2N$, where N is an integer. Using MATLAB, the distances between troths in the truncation-dominated region($\sigma \sim 0.004$) was found to be $\pi/3 \times (c/\omega_p)$ to within 2 significant figures. The factor of three is expected, as the truncation is at 3σ and therefore increasing σ by x increases the length between the two truncations by 3σ.

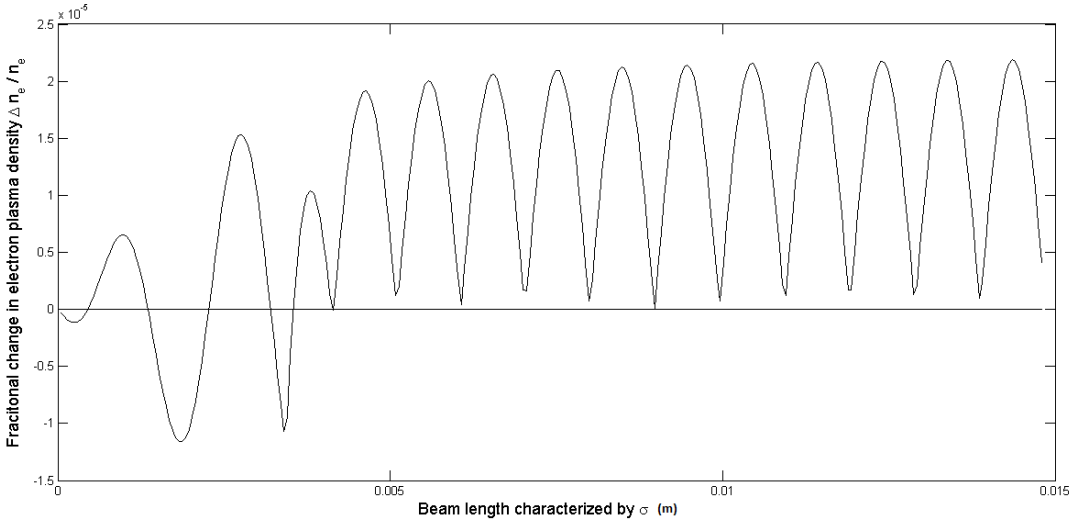

Figure 2.5: Difference in wakefield amplitude profiles between truncated and non truncated models 2.26 2.32 as function of beam length

2.3 Non-linear Waves

There is another regime to be considered for proton driven plasma wakefield acceleration, and that is when the charge density of the beam is approximately equal to, or greater than the charge density of the plasma electrons. In this regime non-linear effects come to dominate. When the charge density of the beam approaches or exceeds the charge density of the plasma non linear behaviour is exhibited. The plasma electrons move relativistically, so the plasma frequency, ω_p, is modified by a lorentz factor, γ, 2.33 and the resonance condition of $L_b = \lambda_p/2$, where L_b is the length of the beam, is shifted.

$$\Omega_p = \frac{n_e e^2}{\gamma \epsilon_0 m_e} = \frac{\omega_p^2}{1+\Phi} \tag{2.33}$$

Also, the perturbation of the background electron density becomes as great as the background electron density itself, and since negative densities are non-physical, the system reacts instead by having larger regions of near zero electron density, followed by sharp peaks of very high electron density 3.11. The high density peaks have an increased local plasma frequency and the driving beam must be shorter to resonantly excite the plasma. This density profile can no longer be described by a simple sinusoid and requires a different mathematical approach **??**:

Starting with the continuity equation:

$$\frac{\partial n_e}{\partial t} + \frac{\partial (n_e v_x)}{\partial x} = 0 \tag{2.34}$$

Where $v_x = p_x/\gamma m$ is the longitudial velocity and p_x is the longitudinal momentum.

In the general case where the plasma can be driven by a laser or a charged particle beam we can write γ as:

$$\gamma^2 = 1 + \frac{p_x^2}{m^2c^2} + \frac{e^2A^2}{m^2c^4} \tag{2.35}$$

Where the vector potential $\mathbf{A_r} = \mathbf{p_r}c/e$ describes the contribution to the electromagnetic fields by the laser pulse.

The equation for the longitudinal momentum is:

$$\frac{\partial p_x}{\partial t} = e\frac{\partial \phi}{\partial z} - mc^2\frac{\gamma}{\partial z} \tag{2.36}$$

Where ϕ denotes the electrostatic potential. Here the $\partial\phi/\partial t$ term is the electrostatic field and the $\partial\gamma/\partial z$ is the ponderomotive force from the laser. Also, we will need Poisson's equation:

$$\frac{\partial^2\phi}{\partial z^2} = \frac{e}{\epsilon_0}(\Delta n_e + (sign?)n_b - n_0) \tag{2.37}$$

Where n_b is the proton number density of the driving beam. Applying the quasi-static approximation. 2.36 becomes:

$$e\phi = (\gamma - 1)mc^2 - cp_x \tag{2.38}$$

Redefining the potentials in dimensionless form: $\Phi = e\phi/mc^2$ and $\mathbf{a} = e\mathbf{A}/mc^2$ and applying the quasi-static approximation, we find a single wakefield equation:

$$\frac{\partial^2 \Phi}{\partial \zeta^2} = \frac{1 + \mathbf{a}^2}{2(1+\Phi)^2} - \frac{1}{2} + \frac{n_b}{n_0} \tag{2.39}$$

2.4 Efficiency

Perhaps the biggest limitation of particle driven plasma wakefield acceleration is the transformer ratio 2.40. There is a upper limit to the maximum energy gained by the witness beam, which is twice the energy of the driving beam.

$$R = \frac{E_{witness\ max}}{E_{drive\ max}} \leq 2 - \frac{N_{witness}}{N_{drive}} \tag{2.40}$$

Where $E_{drive\ max}$ is the maximum electric field of the drive beam, $E_{witness\ max}$ is the maximum electric field acting on the witness beam, $N_{witness}$ is the number of particles in the witness beam and N_{drive} is the number of particles in the driving beam. When the second half of the beam acts to fully reinforce the oscillation established by the first half, $2E_{drive} = E_{witness}$, and when the number of particles in the witness beam is far less than the driving beam, $N_{witness}/N_{drive} \sim 0$, and the transformer ratio is at its maximum value of 2. This transformer ratio applies to longitudinally symmetric beams and can be overcome with non-symmetric beams [17], but this would be a technical challenge. Another method of increasing the energy gain of the witness beam above a factor of two is to use multiple driving beams to cumulatively increase the amplitude of the wakefield [18]. When the driving beams are spaced π apart they all lose energy to the wakefield at the same rate and the multi-beam transformer ratio becomes $R_{multi} = M \times R$, where M is the number of driving beams.

2.5 Self modulation of long proton beams

The SPS beam at CERN is best described by a long Gaussian beam ($L > \lambda$) relative to useful plasma densities - as discussed in the introduction 3.13. A long beam described by a Gaussian profile will not efficiently produce a wakefield directly, but there is a modulation effect which enables them to excite the wakefield to high amplitudes. The head of the beam begins to generate a wakefield within the body of the beam. Consider the first plasma electron peak generate within the beam. It will act to pull the local protons in the beam towards it, whilst the adjacent regions of ions act to push the proton beam away from them, effectively cutting the first $\lambda/2$ of the beam from the rest. The remaining beam then sets up a wakefield within itself and the process repeats, modulating the beam at the plasma frequency. This leads to positive

feedback and and unstable modulation of the whole beam, effectively cutting the beam into multiple short pulses. These pulses will be spaced $\sim \pi$ apart and will each act to increase the magnitude of the wakefield, which attains an amplitude of oscillation many times greater than any single pulse could.

3 Data Analysis and Discussion

This section first familiarises the reader with 1D simulations in OSIRIS, the form of the output and potential pitfalls and phenomena. Then it goes on to examine beam length parameter scans over σ to find the length at which a Gaussian beam resonantly excites the plasma. Finally a more detailed 2D cylindrical simulation of a the Super-Proton-Synchrotron beam at CERN will be examined and its potential to be used for PD-PWA is investigated.

3.1 1D Simulations In OSIRIS

3.1.1 A Typical 1D Simulation

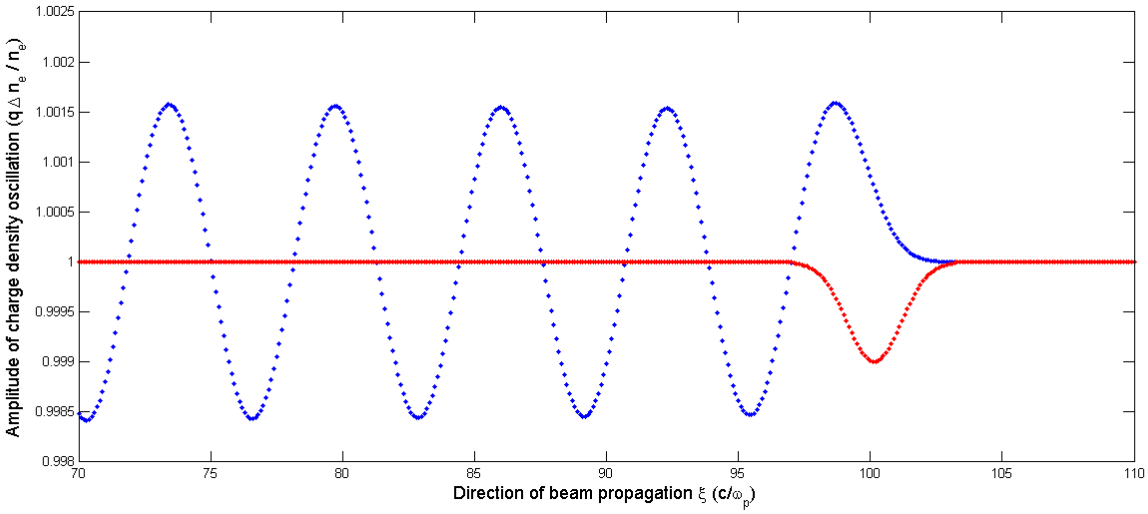

Figure 3.1: 1D OSIRIS simulation of plasma electron response (blue) to a proton driving beam (red) where $\sigma = (13\pi/40) * (c/\omega_p)$ and the number density of the beam is $n_{b\ peak} = n_e/1000$

Figure 3.1 is a typical data dump of a 1D simulation. The blue line shows the variation in the plasma electron charge density and the red line shows the proton driver beam. Note that the proton driver beam has been shifted up by 1, so both plots could be shown together. The size of the simulation box

is 150×3 cells and co-moves with the beam. The beam is propagating to the right. To the right of the beam is the unperturbed cold plasma and to the left is the resulting wakefield. After a certain number of time steps the data dumps evolve to a point where they are largely unchanging, this is when the quasi-static approximation applies. The beam has a Gaussian profile described by equation 3.1.

$$n_{b_\xi} = e^{-\left(\frac{\xi}{\sqrt{2}\sigma}\right)^2} \tag{3.1}$$

and has a number density of $0.001 \times n_e$ at its centre. Also the Gaussian beam has $\sigma = 0.4710(c/w_p)$ and is set to zero at $3 \times \sigma$ from the centre of the gaussian for computational purposes. The energy of the proton beam is $E = 450GeV$, which is high enough to remain relativistic after significant energy loss.

One assumption that can quickly be checked is that the ions' response to the driving beam is negligible compared to the electrons response, and thus can be considered static. This assumption was used to derive equation 1.1.

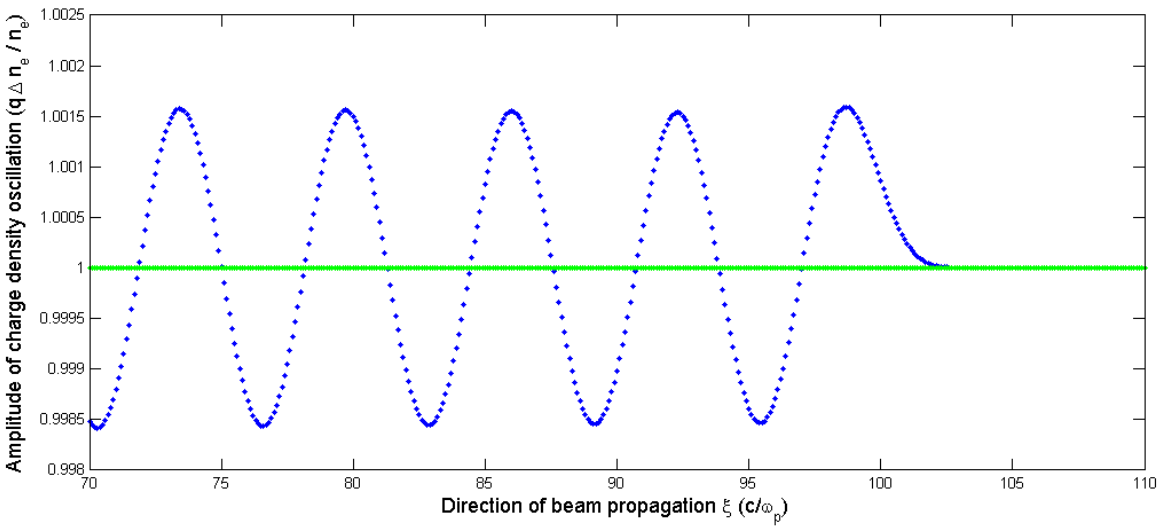

Figure 3.2: Plasma's electron and ion response to proton driver beam

Figure 3.2 shows the same simulation as figure 3.1, where the plasma electrons response in blue and the plasma ions response in green. The amplitude of density oscillation for the electrons is $0.0037 \times n_p$ where as the amplitude of density oscillation for the ions is $2.77 \times 10^{-6} \times n_p$, over three orders of magnitude lower. Therefore the assumption that the ions remain static is a reasonable one.

3.1.2 Maintaining Pseudo 1D Symmetry

OSIRIS currently has no implemented 1D co-ordinate system, so a 2D Cartesian system with 1D symmetric initial conditions was used for the pseudo-1D simulations. It was discovered early on that the simulations' 1D symmetry breaks down several λ_p behind the beam if certain conditions are not met. Namely the resolution, number of particles per cell and the correct choice of boundary conditions. Broken 1D simulations are presented and contrasted against simulations with improved resolution/particles per cell and minimum requirements for maintaining 1D symmetry are found.

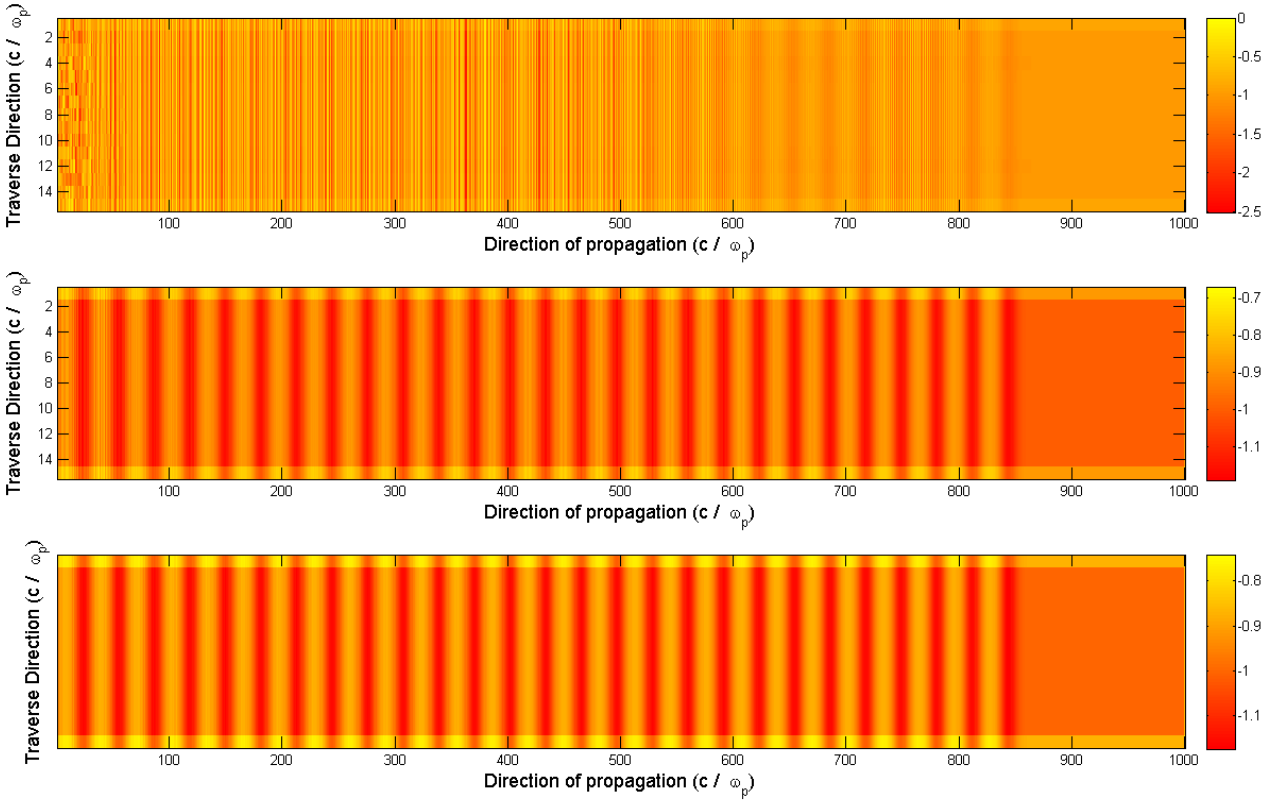

Figure 3.3: Three data dumps three simulations, at the same time step, that only differ by resolution. The top, middle and bottom plots have resolution of 2.5, 10 and 15 respectively

Figure 3.3 shows the effect of resolution on 1D symmetry breaking. The three data dumps are from three different simulation at the same time step. Each simulation has a simulation box size of 200×15 but varying spacial grid sizes. The top plot in Figure 3.3 has a spacial grid size of 500×15, the middle

2000×15 and the bottom 3000×15. The resolution is calculated by dividing the spacial grid size by the simulation box size and is 2.5×1, 10×1 and 15×1 for the top, middle and bottom respectively. To the right of the top plot the 1D symmetry has broken, furthermore the wakefield in the x direction also breaks down soon after it is established. The middle plot shows no 1D symmetry breaking, but there is still wakefield breakdown. The bottom plot shows no sign of 1D symmetry breaking and very little distortion to the established wakefield. For this reason a resolution of 10 is used in both the x and the y direction in all further simulations.

3.1.3 OSIRIS Anomaly

Replotting figure 3.1, one can see that the amplitude of the wakefield increases from right to left.

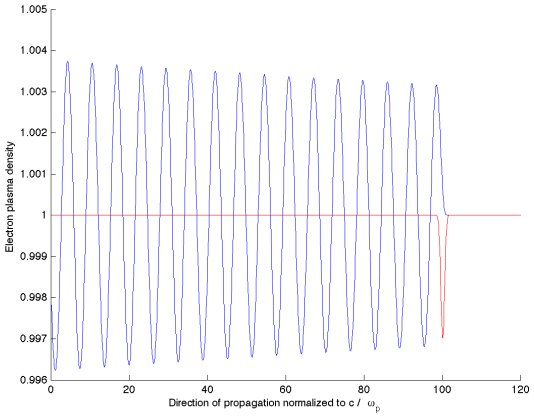

Figure 3.4: Re-plot of figure 3.1. A 1D OSIRIS simulation of plasma electron response (blue) to a proton driving beam (red) where $\sigma = (13\pi/40) * (c/\omega_p)$ and the number density of the beam is $n_{b\ peak} = n_e/1000$

The amplitude of the wakefield between $0 - 10$ is a factor of 1.174 larger than the initial amplitude of the wakefield. Either the amplitude of oscillation, once set by the beam, is increasing with time; or the beam spreads out as it travels through the plasma, lowering its peak density and therefore the amplitude of the resulting wakefield. Figure 3.5 plots the beam over a range of time steps to investigate the latter.

Figure 3.5 shows the driving beam that created the wakefield in 3.4 at 6 different time steps, 1000 time steps apart, plotted in red, blue, green, cyan, magenta and black. However, all the beam profiles are the same and sit on top of each other, making only the black plot visible. From this we can see that

Figure 3.5: Proton beam that excited the plasma in figure 3.4 at different time steps

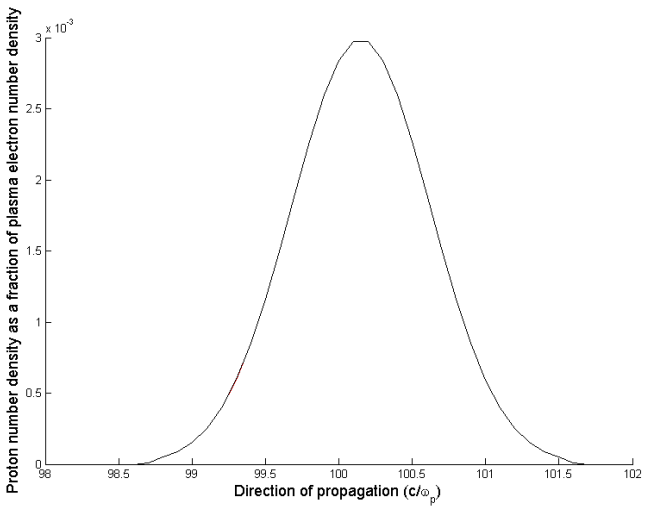

the peak density does not change over these time scales and therefore can not explain the change in wakefield amplitude seen in figure 3.4.

Figure 3.6 plots the same simulation at two different time steps, both centred on the driving beam, to investigate the former.

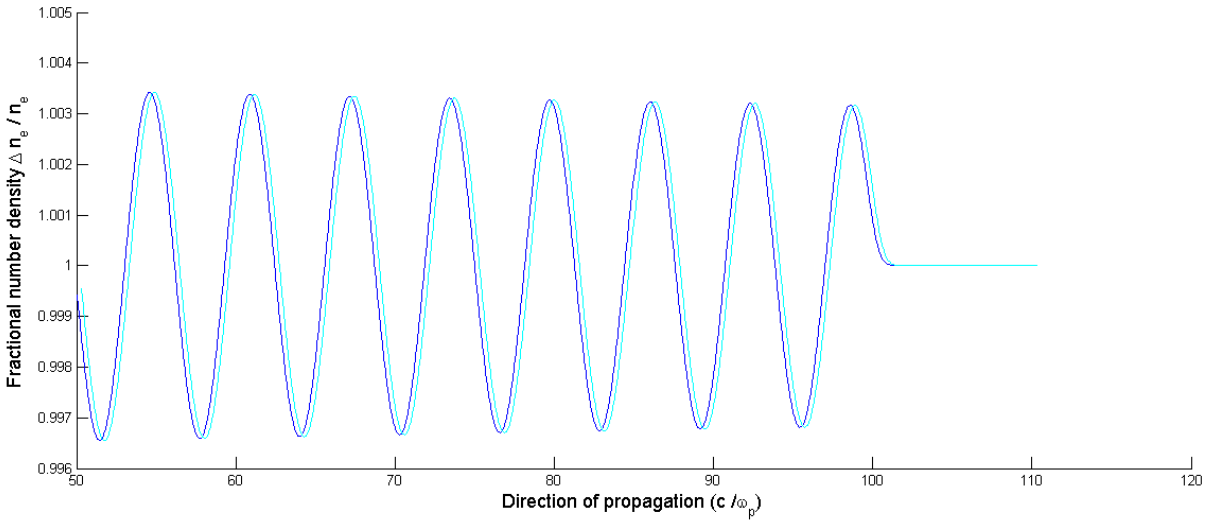

Figure 3.6: The resulting plasma electron wakefield at two different time steps

Figure 3.6 shows two data dumps from the same simulation as described by figure 3.4, 5000 time steps apart, where a time step is normalised to $(0.009 \times 1/\omega_p)$. The later data dump (cyan) actually sits exactly on top of the earlier time step (blue) but has artificially been shifted for demonstration purposes.

As seen, the later time step still creates the same initial amplitude wakefield as the earlier time step. Furthermore, both show the exact same wakefield amplitude increase once the beam has passed. So the amplitude of the resulting wakefield is in fact growing with time. One possible source of energy for this growing oscillation is from the oscillation of the more massive ions. Figure 3.7 shows the small amplitude wakefield established in the ions from the same simulation and timestep as figure 3.4.

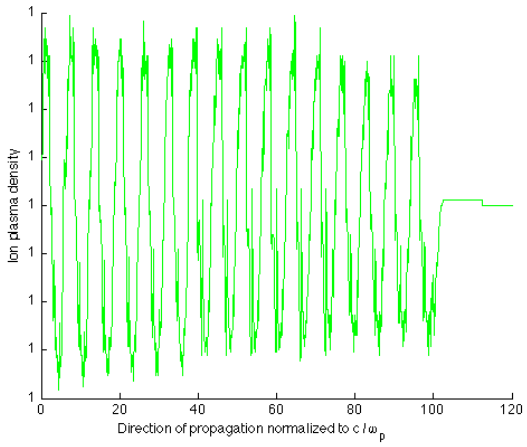

Figure 3.7: The resulting plasma ion wakefield at two different time steps

As seen in figures 3.4 and 3.7 the wakefield of both the ions and electrons grow with time. This is a non-physical result as there is no source of energy for the wakefield to draw from once the beam has passed. This error can be put down to numerical rounding issues of the OSIRIS code, and is important to highlight as the true amplitude of the wakefield to be measured is that of the initial wakefield, not that of the later error-amplified wakefield.

3.1.4 Low Density Beam Length Parameter Scans

Parameter scans of σ, characterising beam length, were run for numerous 1D low density proton beam-plasma interactions in order to find the value of σ for a Gaussian density profile beam to resonantly excite the plasma and to see if the variable charge truncated Gaussian model 2.32 agrees with the simulations. A template input deck was used for each batch of simulations, the details of which can be found in table .2. The full input deck is found in the appendix A. The details of each batch/parameter scan can be found in table 3.2. Note that the beam length is characterised by σ.

The beam is centred at $x = 80$, with the cold hard-edged plasma starting at $x = 130$ and the simulation box moving at c in the x direction following the

Parameter	Value
Spatial grid	1300(x) 30(y)
Simulation box	130(x) 3(y)
Particles per cell	16 (4x, 4y)
Time step $(1/\omega_p)$	0.009 dt
Dump (time step)	1000
Beam composition	Proton
Beam profile	Truncated Gaussian
nsigm (σ)	3
Beam energy	450GeV
Plasma electron number density	1 $(m_e\epsilon_0\omega_p^2/e^2)$
Plasma ion number density	1 $(m_e\epsilon_0\omega_p^2/e^2)$

Table 3.1: 1D-Simulation Parameters

Parameter scan	Beam density $n_{b\ peak}/n_e$	Initial $\sigma(c/\omega_p)$	σ iteration size (c/ω_p)
Batch A	0.01	$\pi/40$	$\pi/40$
Batch B	0.003	$\pi/40$	$\pi/40$
Batch C	0.001	$\pi/40$	$\pi/40$
Batch D	0.0003	$\pi/40$	$\pi/40$
Batch E	0.0001	$\pi/40$	$\pi/40$
Batch F	0.000001	$\pi/40$	$\pi/40$

Table 3.2: Parameter scans over σ for low density gaussian proton beams

beam as it travels through the plasma. nsigm is a key quantity whose impact is examined in 3.8. It determines after how many $\sigma's$ from the centre of the Gaussian the density is artificially set to zero. Gaussian functions extend to $\pm\infty$ and it is a necessary computational fix to truncate them. Choosing high values for nsigm include more of the Gaussian but require bigger simulation boxes and longer run times to accommodate them. A value of nsigm $= 3$ was chosen as it encompasses 99.7% of the particles in the beam whilst keeping the amplitude of the Gaussian at the artificial hard edge at a modest 1.11% of the central density. This low amplitude hard edge was found to still have a detectable affect as shown in figure 3.8.

Figure 3.8 shows the amplitude of wakefield oscillation vs beam length for Gaussian beams truncated at different points. The red data points are for a Gaussian truncated at $\sigma = 1$, green truncated at $\sigma = 2$ and blue truncated at $\sigma = 3$. With relative densities at the hard-edged truncation of $n_{b_{trunc}}/n_{b_{peak}} = 0.607$, $n_{b_{trunc}}/n_{b_{peak}} = 0.135$ and $n_{b_{trunc}}/n_{b_{peak}} = 0.0111$ respectively.

Simulated data inherently has no measurement error. The OSIRIS anomaly's effect mentioned earlier, where the amplitude of the wakefield increased with

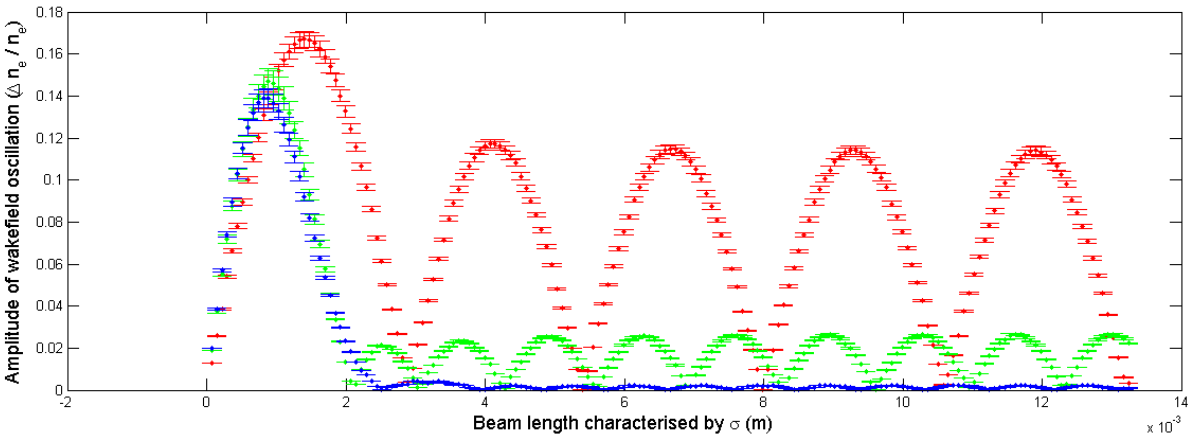

Figure 3.8: Three beams of density $n_{b_{max}} = 0.003 \times n_e$ truncated at $\sigma = 1, 2, 3$ for red, green, blue respectively

time, could not be completely nullified as the fitting tool used needed a range of data points to properly extract the amplitude, and the wider the range the more error amplified data points were counted. This is why the error bars are present and they represent a 95% confidence interval.

Figure 3.8 shows the lesser peaks predicted by the truncated variable charged model 2.32. Furthermore it shows that the amplitude of the lesser peaks increases as the points of truncation move closer to the central peak of the Gaussian. In fact the amplitude of these lesser peaks increases linearly with the amplitude of the density of the beam at truncation as shown in figure 3.9, albeit with only three data points.

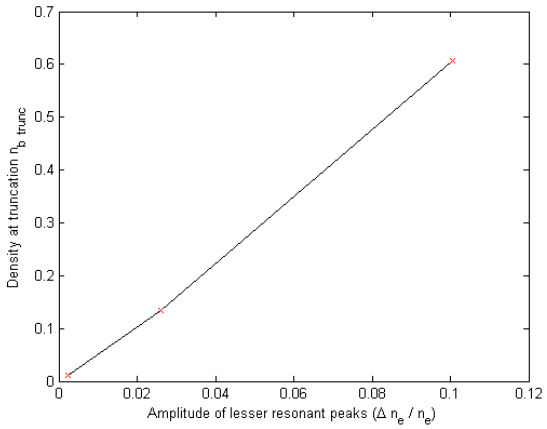

Figure 3.9: Amplitude of lesser resonant peaks vs Fractional beam density at hard-edged truncation

The resonance profiles in figure 3.8 are essentially a superposition of a Gaus-

sian beam resonance profile with a lower density hard edge constant beam resonance profile. Note that the distance between lesser peaks of the nsigm = 1 (red) is twice that of the nsigm= 2 (green) and three times that of the nsigm= 3 (blue). This is a result of the hard-edged component of the three sets of beams being longer as nsigm is increased. The higher the value of nsigm of a beam, the greater the length of its hard edge component and the quicker that component falls in and out of resonance with the plasma as σ is increased.

Figure 3.10 compares the amplitude wakefield profile as a function of σ for simulated data against the variable charge truncated Gaussian beam model. The model fits the data well for short ($\sigma < 0.4(c/\omega_p)$) and long ($\sigma > 1(c/\omega_p)$) beam lengths, and diverges by a maximum factor of 1.0138 as the beam length reaches resonance. If this divergence is physical, then the maximum energy gain This divergence is minimised as the range over which the fitting tool acts is reduced and is a result of the OSIRIS anomaly discussed earlier. Also, the model's prediction of lesser peaks at high beam lengths agrees with the simulated data and matches the first two peaks very closely. Further more it has been established theoretically and via simulations that the resonance condition in the linear regime is that given by equation 2.30. In summary the variable charge truncated Gaussian model 2.32 accurately predicts the amplitude of the wakefield established by a Gaussian proton beam perturbing a cold plasma. Furthermore the model can be generalised to a Gaussian truncated at any point by changing the integration limits of equation **??** to $\pm\tau$, where τ is the desired point of truncation from the centre, Allowing the model to represent a wider range of beam profiles.

3.1.5 High Density Beam Length parameter Scans and Non-linear frequency shift

Parameter scans of beam length were run for 1D high density proton beam-plasma interactions ($n_b\ n_p$) to characterise the non-linear response of the plasma and explore at which densities non-linear effects come to dominate. The value of σ that causes a Gaussian high density beam to resonantly excite the plasma is investigated. The details of these simulations can be found in table **??**.

Batch name	Beam density (n_{bmax}/n_p)	Initial $\sigma(c/\omega_p)$	σ iteration size (c/ω_p)
Batch G	0.1	$\pi/40$	$\pi/40$
Batch H	0.3	$\pi/40$	$\pi/40$
Batch I	1	$\pi/40$	$\pi/40$

Figure 3.11 shows a non-linear response to the high density driving beam.

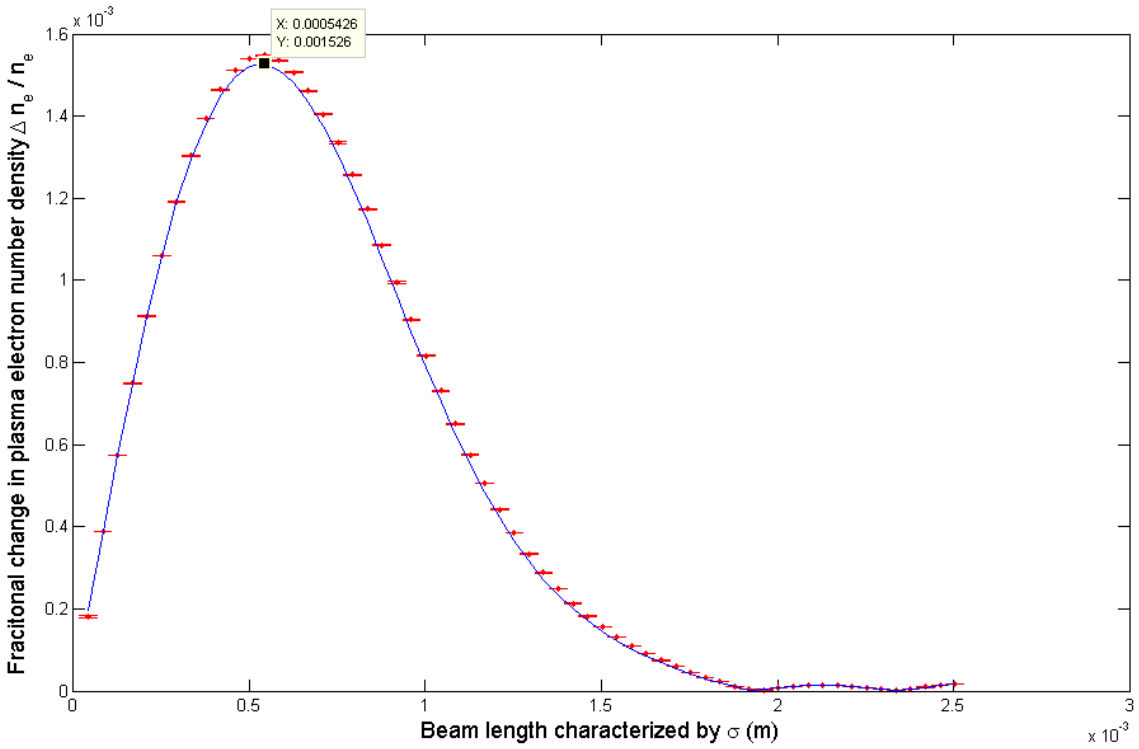

Figure 3.10: The amplitude of wakefield oscillation as a function of σ for 1D simulations (Batch C 3.2) of Gaussian density profile beams of peak number density $n_b = n_e/1000$ (red) and for the variable charge truncated Gaussian beam model (blue) 2.32

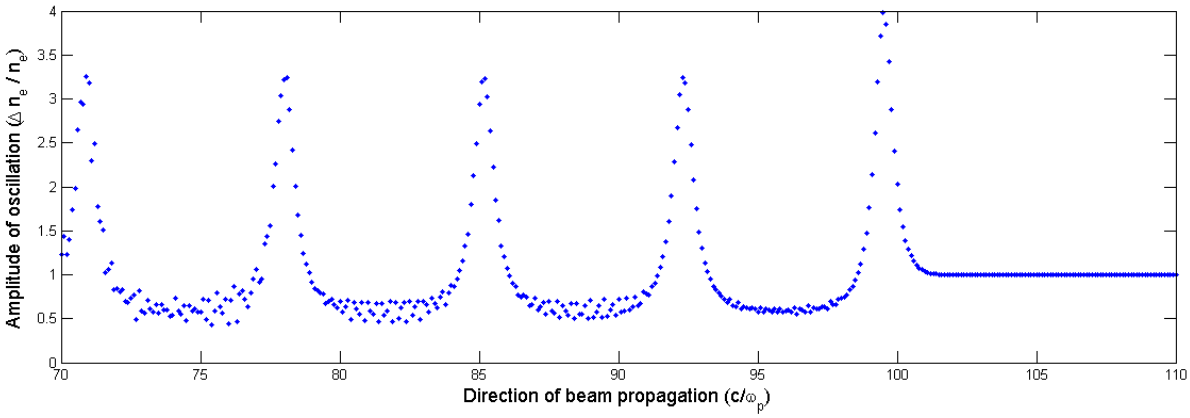

Figure 3.11: Data dump of $n_b/n_p = 1$ 1D simulation at resonance ($\sigma = 8\pi/40$) showing saw-tooth electron plasma density profile

The response is no longer sinusoidal density profile, but a saw-tooth electron density profile. This is a result of the driving beam pulling electrons in from

wider regions as its number density is increased. Note that the wakefield destabilises over a smaller number of λ_p compared to the linear regime.

Figure 3.12 shows the amplitude of the wakefield as a function of σ for three sets of high density beams. The red data points are for beams of density $n_b/n_p = 1$, green $n_b/n_p = 0.3$ and blue is for $n_b/n_p = 0.1$. The blue wakefield amplitude profile peaks at $\sigma = 0.862(c/\omega_p)$, shifted below the resonance condition of the linear regime of $\sigma = \sqrt{2}(c/\omega_p)$. The green wakefield amplitude profile is shifted even greater to $\sigma = 0.706(c/\omega_p)$ and the red profile peaks at $\sigma = 0.549(c/\omega_p)$. The nonlinear effects are not limited to shifting the resonance peaks, but also generate lesser peaks of decreasing amplitude. Figure 3.12 demonstrates that non-linear effects impact the resonance condition with beam densities as low as $n_b/n_p = 0.1$, in the next section the SPS beam is simulated at peak beam densities far lower than this value and well within the linear regime.

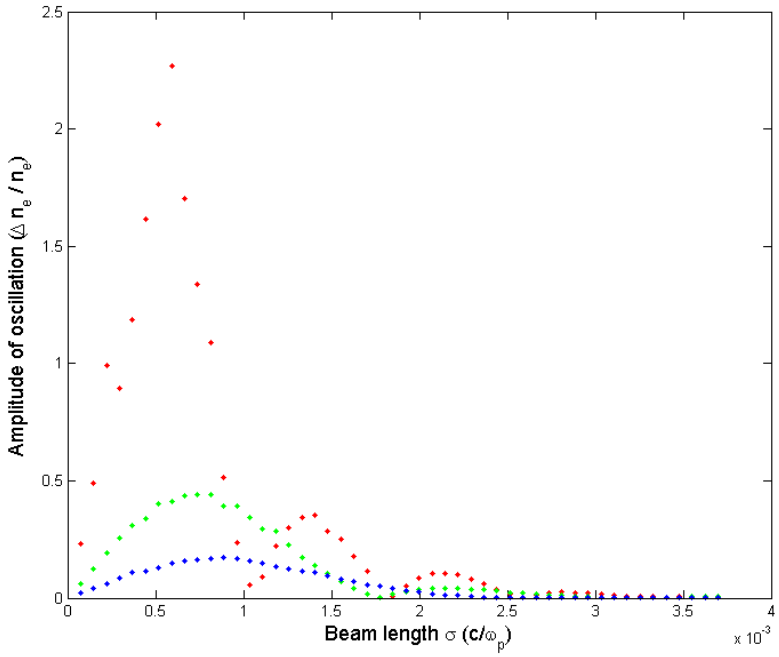

Figure 3.12: Wakefield Amplitude plotted against beam length, σ, for high density batches G, H, I. Absolute measurement of wakefield amplitude.

3.2 2D-Simulations

There are a number of institutes with interest in PD-PWA .1 and the parameter sets in table 3.13 and beam profile for the SPS beam in equation 3.2 have been issued for easy comparison of simulations. The 2D cylindrical SPS simulation was run with set 3 parameters and ran for a total of 256,000 time steps, which corresponds to a physical time of 144 nano seconds. In this time the beam propagated through the full 10 meters of plasma. The initial peak beam density is $n_b/n_e = 0.00132$ so one would expect a linear response by the plasma. However, the length of the beam is 109.1 times longer than the plasma wavelength and self modulation effects may cause a large non-linear wakefield to form. The simulation was run with with a spacial grid of 6000(z) by 100(r) and a simulation box size of 1200(z) by 20(r) and a resolution of 5(z) by 5(y). The lower resolution was a necessary compromise to get the simulation run time down. The number of particles per cell was 3(z) 3(r).

	PS	PS	SPS 'LHC Bunch'	SPS 'LHC bunch'	SPS 'Totem bunch'
Parameter	Set 1	Set 2	Set 3	Set 4	Set 5
$E_p(GeV)$	24	24	450	450	450
$N_p(10^{10})$	13	13	11.5	11.5	3
$\sigma_p(MeV)$	12	12	135	135	80
$\sigma_z(cm)$	20	20	12	12	8
$\sigma_r(\mu m)$	400	400	200	200	100
$\sigma_\theta(mrad)$	0.25	0.25	0.04	0.04	0.02
$n_0(cm^{-3})$	10^{14}	3×10^{14}	10^{14}	10^{15}	10^{15}
$L_p(m)$	10	10	10	10	10

Figure 3.13: Parameter Sets for 2D cylindrical SPS beam simulations

$$n_p = \frac{N_p}{2\sigma_r^2\sigma_z(2\pi)^{3/2}} e^{-r^2/2\sigma_r^2} \left(1 + \cos\left(\sqrt{\frac{\pi}{2}}\frac{z}{\sigma_z}\right)\right) \tag{3.2}$$

Here, E_p is the energy of the proton beam, N_p is the number of particles in the beam, σ_p is the energy spread of the beam, σ_z is the longitudinal spread of the beam, σ_θ is the divergence of the beam, n_0 is the plasma density and L_p is the length of the plasma through which the beam is to be simulated. This density profile is sinusoidal in the x direction and falls to zero at $z = \pm\sqrt{2\pi}\sigma_z$ and is limited to this range. It is Gaussian in the radial direction and of constant charge.

Figure 3.14 plots the beam profile described by equation 3.2 at time $t = 0s$. Figure 3.15 takes this initial beam profile and subtracts the final beam pro-

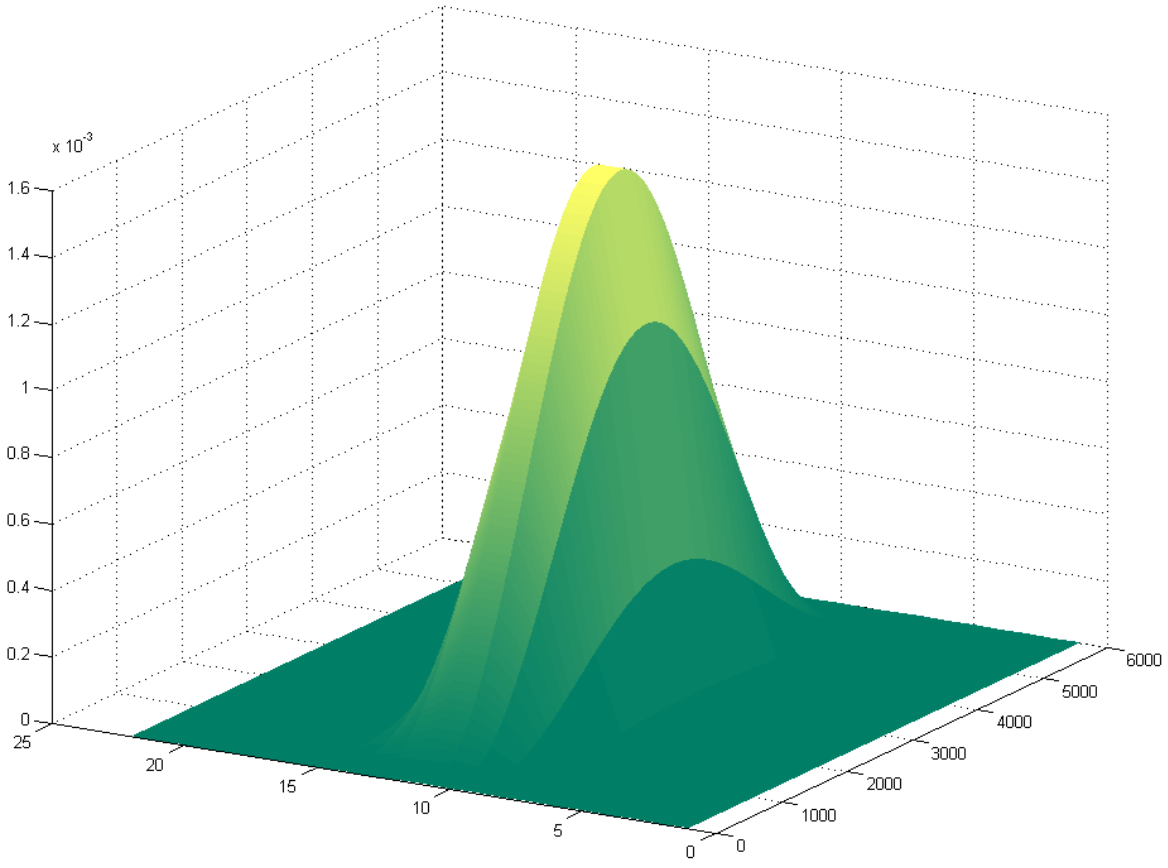

Figure 3.14: The SPS beam profile described by equation 3.2 and set 3 parameters from table 3.13. The axis spanning 0 to 6000 is increasing in the direction of propagation and one unit is $1/(5 \times \kappa_p)$ meters. The axis spanning 0-20 is in the radial direction, where the centre of the beam sits at r = 0 and one unit is $1/(5 \times \kappa_p)$ meters. The axis spanning 0-1.6 $\times 10^{-3}$ is the proton charge number density

file at time $t = 144 \times 10^{-9} s$ in order to highlight any self modulation effects. No change of any kind is found and the beam remains unchanged. No self modulation effect has taken place and no thermal spreading of the beam has occurred over the 144 nano seconds.

Figure 3.16 shows the plasma's response after 144 nano seconds. The plasma is largely unperturbed until the beam has almost completely passed, at which point it exhibits non-linear behavior and the amplitude of oscillation rises dramatically, peaking at $\Delta n_e/n_e = 1.186$. Figure 3.17 examines this maximum peak closer.

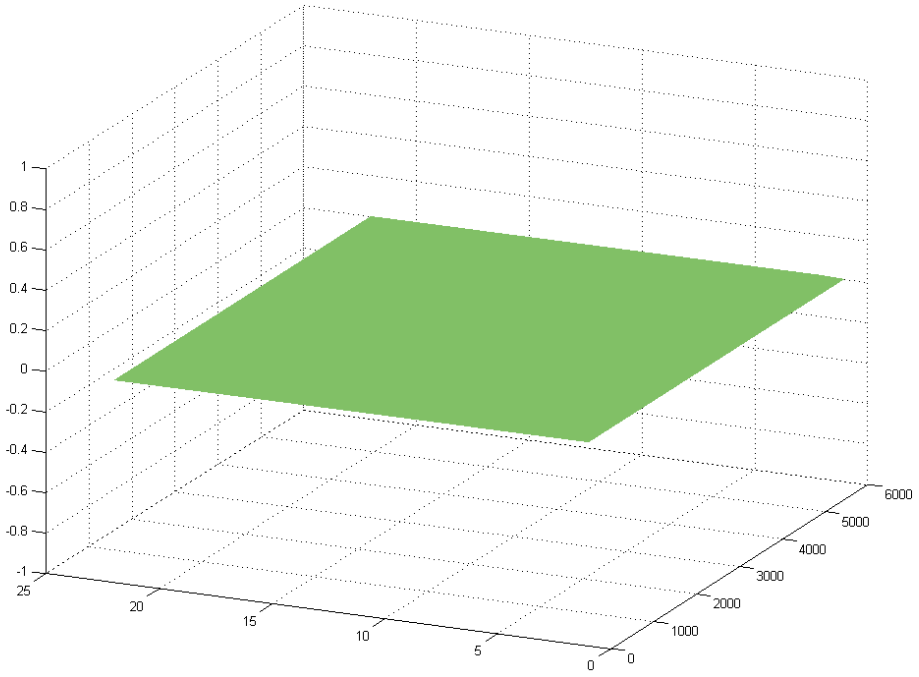

Figure 3.15: The difference between the SPS beam at $t = 0$ as seen in figure 3.14 and the final beam at $t = 144 \times 10^{-9}s$ The axis spanning 0 to 6000 is increasing in the direction of propagation where one unit is $1/(5 \times \kappa_p)$ meters. The axis spanning 0-25 is in the radial direction, where the centre of the beam sits at r = 12 and one unit is $1/(5 \times \kappa_p)$ meters. The axis spanning -1 to 1 is the proton charge number density

The profile of the wakefield seen in figure 3.17 is characteristic of the low resolution simulations seen in 3.3. The middle plot of figure 3.3 has the same resolution as the 2D SPS simulation and has minor disruptions (seen as striations) to its wakefield after 200 grid cells of wakefield propagation. The 2D SPS simulation has a simulation box that is 1200 grid cells long, and therefore a longer amount of time for any resolution induced disruptions to propagate. This, taken with the lack of self modulation, introduces doubt that the high amplitude oscillations seen at late times towards the back of the simulation box are a physical result. In either case, the quality of the wakefield at late times would produce a low quality witness beam with a wide energy spread. The lack of self modulation can be explained by the lack of a hard edge. A hard edge introduces a sudden force - as the cold plasma electrons do not see the field of the beam until it arrives due to the field co-moving with the beam

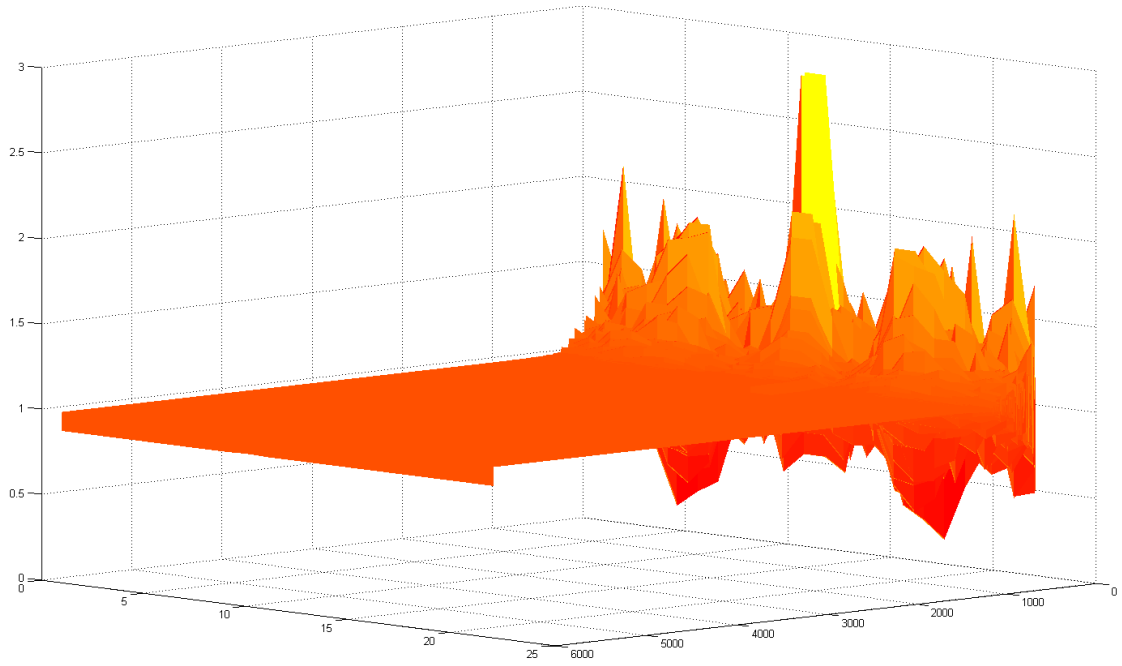

Figure 3.16: The plasmas' response to the Gaussian beam seen in figure 3.14. The axis spanning 0 to 6000 is increasing in the direction of propagation where one unit is $1/(5 \times \kappa_p)$ meters. The axis spanning 0-25 is in the radial direction, where the centre of the beam sits at r = 12 and one unit is $1/(5 \times \kappa_p)$ meters. The axis spanning $0 - 3$ is the proton charge number density

at c. This sudden force creates an initial high amplitude wakefield which disrupts the body of the beam. A soft edge beam creates a low amplitude wakefield which cannot modulate the beam over the time scales discussed. This being said, there is a smoother, lower amplitude wakefield that propagates through most of the simulation box as seen in figure 3.18. The wakefield is on the limit of what OSIRIS is able to resolve, the hard edged steps are not a result of a low spacial resolution, but instead of the fact that the oscillation is of such a low amplitude. Each step corresponds to a fractional density change of $(\Delta n_e/n_e = 0.0000004)$

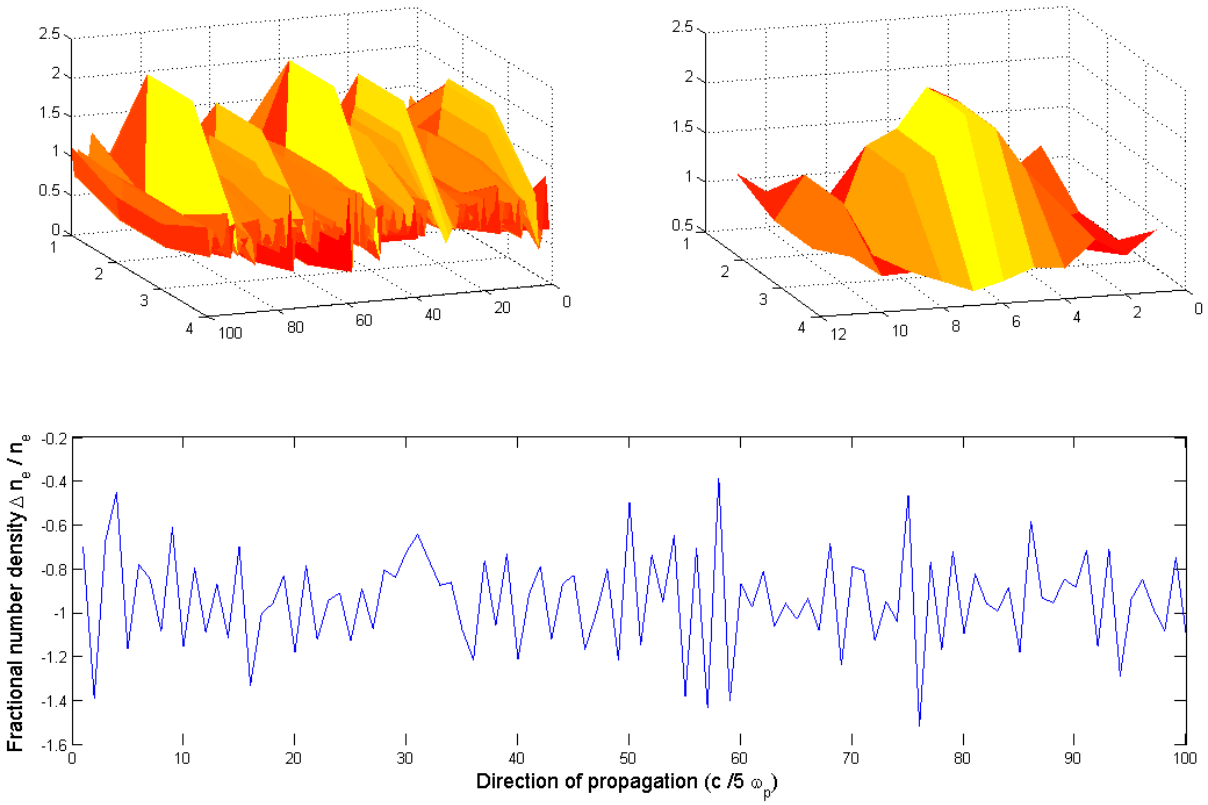

Figure 3.17: The Top left plot shows the first 100 cells of high amplitude oscillation, as seen in figure 3.16. The top right plot then shows wake siting at $z = 30$. The bottom plot shows the amplitude of oscillation along the axis of propagation. The axis spanning 0 to 100 is increasing in the direction of propagation where one unit is $1/(5 \times \kappa_p)$ meters. The axis spanning 0-1 is in the radial direction, where the centre of the beam sits at r = 2.5 and one unit is $1/(5 \times \kappa_p)$ meters. The axis spanning 0-1.6 $\times 10^{-3}$ is the proton charge number density

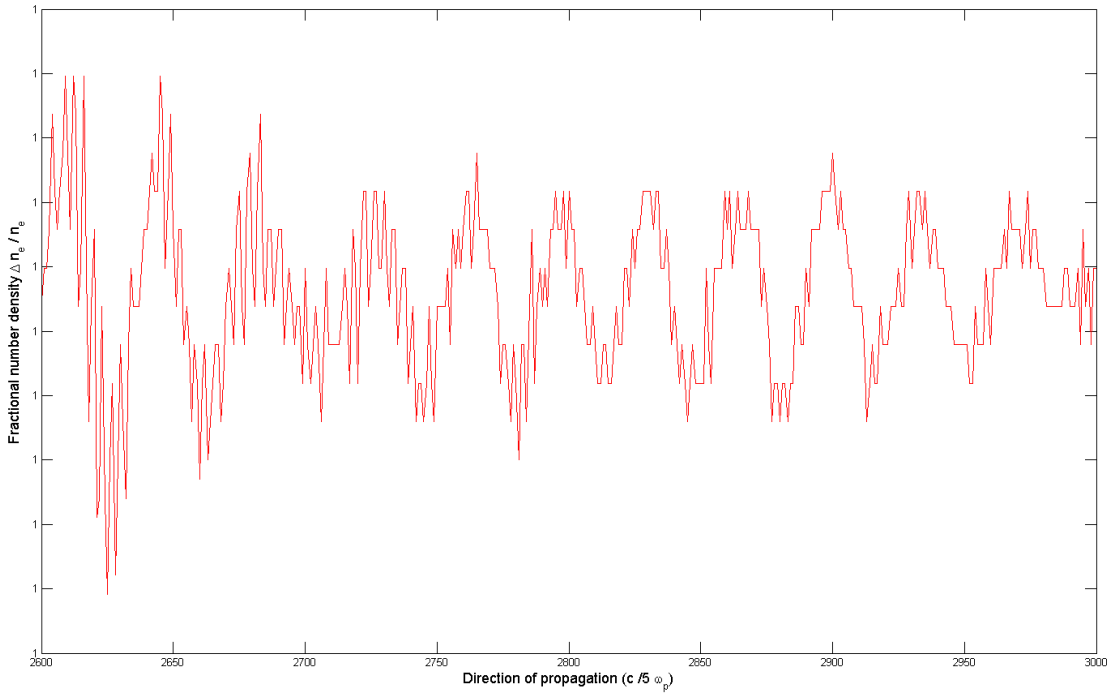

Figure 3.18: This is a crop between 2600 to 3000 of the 6000 data points along the axis of propagation and shows a low amplitude wake-field. Each 'step' corresponds to a fractional density change of $(\Delta n_e/n_e = 0.0000004)$.

4 Conclusions

To conclude, the variable charge Gaussian beam model predicts wakefield oscillation amplitudes that agree with simulated data over the linear regime. The resonance condition for a Gaussian beam was found and the effects of beam truncation explored.

The 2D simulation of the untreated SPS beam revealed a lack of self modulation and produced a noisy, high amplitude, low quality wakefield. Longer simulations of higher resolution and run time may shed light on whether the self modulation effect would eventually dominate and whether the quality of the wakefield is also a result of the resolution of the simulation. The simulation suggests that the SPS beam would be unsuitable for plasma wakefield acceleration, although the high amplitude of the plasma oscillation does suggest that there are potentially high energy gains to be made if beam treatment could result in a more stable wakefield being produced.

Further work includes:

- Deriving a model that describes the response of the plasma to a driving beam of any density, i.e. accommodates the non-linear regime and comparison with simulations
- Methods of beam cutting to create a hard leading edge for the SPS beam
- Simulations of a hard-edged, cut, SPS beam to explore the self modulation instability and its effect on the quality and amplitude of the resulting wakefield
- Simulations of multiple resonant length beams fired into the plasma and the effects of positive reinforcement of the resulting wakefields

Bibliography

[1] (13).

[2] Francis F. Chen. *Introduction to Plasma Physics and Controlled Fusion*. Number 7. Springer, second edition, 1984.

[3] Paul H. Rutherford Robert J. Goldston. *Introduction to Plasma Physics*. Taylor and Francis Group, pap/dis edition, 1995.

[4] et al. Power, J. G. The 9th aac workshop. 569(605-615), 2001.

[5]

[6] F. Amiranoff P. Audebert J. C. Gauthier A. Antonetti J. R. Marques, J. P. Geindre and G. Grillon. Temporal and spatial measurements of the electron density perturbation produced in the wake of an ultrashort laser pulse. *Physical Review Letters*, 76(14), 1996.

[7] D. Fisher T. Tajima M. C. Downer A. Babine A. Stepanov C. W. Siders, S. P. L. Blanc and A. Sergeev. Laser wakefield excitation and measurement by femtosecond longitudinal interferometry,. *Physical Review Letters*, 76(15), 1996.

[8] Andreas J. Kemp, J. Fuchs, Y. Sentoku, V. Sotnikov, M. Bakeman, P. Antici, and T. E. Cowan. Emittance growth mechanisms for laser-accelerated proton beams. *Phys. Rev. E*, 75(2):056401, May 2007.

[9] I. Kostyukov, E. Nerush, A. Pukhov, and V. Seredov. Electron self-injection in multidimensional relativistic-plasma wake fields. *Phys. Rev. Lett.*, 103(3):175003, Oct 2009.

[10] Alexander Pukhov Frank Simon Allen Caldwell, Konstantin Lotov. Proton-driven plasma-wakefield acceleration. *Nature Physics*, 1(6):363 – 367, April 2009.

[11] T. Tajima and J. M. Dawson. Laser electron accelerator. *Phys. Rev. Lett.*, 43(4):267–270, Jul 1979.

[12] E. Esarey, C. B. Schroeder, and W. P. Leemans. Physics of laser-driven plasma-based electron accelerators. *Rev. Mod. Phys.*, 81(5):1229–1285, Aug 2009.

[13] Z. Najmudin. High intensity laser matter interaction. (9).

[14] Gwenael J. Fubiani. Controlled electron injection into plasma accelerators and space charge estimates. (10), September 2005.

[15] Chandrashekhar Joshi. Plasma accelerators. *Scientific American*, (11):42–46, September 2006.

[16] P. Sprangle, E. Esarey, and A. Ting. Nonlinear theory of intense laser-plasma interactions. *Phys. Rev. Lett.*, 64(16):2011–2014, Apr 1990.

[17] P. Chen et al. Energy transfer in the plasma wakefield accelerator. *Phys. Rev. Lett*, 56(18):1252, September 1986.

[18] Patric Muggli Igor Pavlishin Igor Pogorelsky Daniil Stolyarov Vitaly Yakimenko Wayne D. Kimura Efthymios Kallos, Tom Katsouleas. Plasma wakefield acceleration utilizing multiple electron bunches. (19), 2007.

5 Appendix

.1 Institutes with Interest in using the SPS Beam for PWA

Institutes that have expressed interest in PD-PWA Cockcroft Institute: Swapan Chattopadhyay Imperial College: Ken Long, Jarolslaw Pasternak, Jrgen pozimski Oxford: (john adams institute): Andrei Seryi, Ken Peach, Simon Hooker RAL / STFC: bob Bingham, Rob Edgecock, Peter Norreys UCL: Jon Butterworth, Alexey Lyapin, Matthew Wing from the debriefing of a meeting concentrated on the simulation results for long beams (citation unavailable)

.2 Template Input Deck for 1D Parameter Scans

The input deck used in the high and low density parameter scans is given below, where line 345 (σ) is scanned over within each batch, and line 343 (peak beam density) is different for each batch.

```
1   [frame=single]
2   ! OSIRIS INPUT DECK
3
4   !COMMENTS
5
6   ! this is a very first simulation with particle beams - more to report later
7   !
8   !
9
10  !INPUT DATA
11
12  !--- this is a new one - I have no documentation --
13  !/ &nl_storage
14  !/
15  !--------------the node configuration for this simulation ----------------
16
```

```
17  node_conf
18  {
19   node_number(1:2) = 4, 1,
20   if_periodic(1:2) = .false., .true.,
21  }
22
23
24  !---------------------- spatial grid -------------------
25
26  grid
27  {
28   nx_p(1:2) = 1500, 30,
29   coordinates = "cartesian",
30  }
31
32
33  !-------- time step and global data dump timestep number ----------
34  time_step
35  {
36   dt = 0.009,
37   ndump = 1000,
38  }
39
40  !---------------- restart information --------------------------
41  restart
42  {
43  ndump_fac = 0, file_name = ' ',
44   if_restart = .false.,
45  }
46
47  !---------------- spatial limits of the simulations -------------
48  !(note that this includes information about
49  !the motion of the simulation box)
50
51  space
52  {
53   xmin(1:2) = 0.000d0, 0.000d0,
54   xmax(1:2) = 150.0, 3.0,
```

```
 if_move = .true., .false.,
}

!----------------- time limits ----------------
time
{
 tmin = 0 , tmax = 200,
}

!----------------- field solver set up ----------------

el_mag_fld
{
 b0(1:3) = 0.0d0, 0.0d0, 0.0d0,
 e0(1:3) = 0.0d0, 0.0d0, 0.0d0,
}

!--------------- boundary conditions for em-fields -------------

emf_bound
{
 type(1:2,1) = 30, 30,
 type(1:2,2) = 5, 5,
}

!---------------- diagnostic for electromagnetic fields ---------------

diag_emf
{
 ndump_fac_all = 1, file_name_all = ' ',
 ndump_fac_ave = 0, file_name_ave = ' ',
 n_ave(1:2) = 1, 1,
 ifdmp_efl(1:3) = .true. , .true. , .true. ,
 ifenv_efl(1:3) = .false. , .false. , .false. ,
 ifdmp_bfl(1:3) = .true. , .true. , .true. ,
 ifenv_bfl(1:3) = .false. , .false. , .false. ,
}
```

```
93
94  particles
95  {
96   num_species = 3,
97  }
98
99  !-------------------- diagnostics for all particles ------------------
100
101 diag_particles
102 {
103  ndump_fac = 1, file_name = ' ',
104  if_particles_all = .false.,
105  gamma_limit = 0.0d0,
106  particle_fraction = 1.0d0,
107 }
108
109
110
111 !----------- information for species 1 -----------------------------
112
113 species
114 {
115  num_par_max = 2000000,
116  rqm = -1.0,
117  num_par_x(1:2) = 4, 4,
118  vth(1:2) = 0.0d0 , 0.0d0 ,
119  vfl(1:2) = 0.0d0 , 0.0d0 ,
120  den_min = 1.d-12,
121  if_unneutralized = .false.,
122  num_dgam = 0,
123  dgam = 0.0,
124  n_sort = 0,
125 }
126
127
128 !-------------- density profile for species 1--------------------
129 !number of points in profile along each direction
130
```

```
num_x
{
num_x = 6,
}

!actual profile data

profile
{
 fx(1:6,1) = 0, 0, 1, 1, 1, 1,
 x(1:6,1) = 0, 150.0, 151.570796327, 153.141592654, 25000.0, 300000.0,
 fx(1:6,2) = 1, 1, 1, 1, 1, 1,
 x(1:6,2) = 0, 20, 40, 70, 100, 250,
}


!-------------- boundary conditions for species 1-------------------

spe_bound
{
 type(1,1) = 5, type(2,1) = 5,
 type(1,2) = 5, type(2,2) = 5,
}


!-------------- diagnostic for species 1 -------------------

diag_species
{
ndump_fac_pha = 1,
ps_xmin(1:2) = 0, 0,            ps_pmin(1:3) = -1, -1, -1,
ps_xmax(1:2) = 150.0, 3.0,      ps_pmax(1:3) = 1, 1, 1,
ps_nx(1:2) = 1500.0, 3.0,       ps_np(1:3) = 400, 200, 200,
 if_x2x1 = .true. ,
 if_p1x1 = .true. ,
 if_p2x1 = .true. ,
 if_p3x1 = .false. ,
 if_p1x2 = .true. ,
```

```
 if_p2x2 = .true. ,
 if_p3x2 = .false. ,
 if_p2p1 = .true. ,
 if_p3p1 = .false.,
 if_p3p2 = .false.,
}


!----------- information for species 2 - H ---------------------------

species
{
  num_par_max = 2000000,
  rqm = 1836,
  num_par_x(1:2) = 4, 4,
  vth(1:2) = 0.0d0 , 0.0d0 ,
  vfl(1:2) = 0.0d0 , 0.0d0 ,
  den_min = 1.d-12,
  if_unneutralized = .false.,
  num_dgam = 0,
  dgam = 0.0,
  n_sort = 0,
}


!-------------- density profile for species 2---------------------
!number of points in profile along each direction

num_x
{
num_x = 6,
}

!actual profile data

profile
{
 fx(1:6,1) = 0, 0, 1, 1, 1, 1,
```

```
 x(1:6,1) = 0, 150.0, 151.570796327, 153.141592654, 25000.0, 300000.0,
 fx(1:6,2) = 1, 1, 1, 1, 1, 1,
 x(1:6,2) = 0, 1.1, 1.3, 2, 2.2, 3,
}



!-------------- boundary conditions for species 2-------------------

spe_bound
{
  type(1,1) = 5,  type(2,1) = 5,
  type(1,2) = 5,  type(2,2) = 5,
}


!-------------- diagnostic for species  2 -------------------

diag_species
{
ndump_fac_pha = 1,
ps_xmin(1:2) = 0, 0,            ps_pmin(1:3) = -0.1, -0.1, -0.1,
ps_xmax(1:2) = 150.0, 3.0,      ps_pmax(1:3) = 0.1, 0.1, 0.1,
ps_nx(1:2) = 1500.0, 3.0,       ps_np(1:3) = 400, 200, 200,
  if_x2x1 = .true.,
  if_p1x1 = .true.,
  if_p2x1 = .true.,
  if_p3x1 = .false.,
  if_p1x2 = .true.,
  if_p2x2 = .true.,
  if_p3x2 = .false.,
  if_p2p1 = .true.,
  if_p3p1 = .false.,
  if_p3p2 = .false.,
}

!----------- information for species 3 ----------------------------


```

```
245  species
246  {
247   num_par_max = 2000000,
248   rqm = 1836.0,
249   num_par_x(1:2) = 4, 4,
250   vth(1:2) = 0.0d0 , 0.0d0 ,
251   vfl(1:2) = 0.0d0 , 0.0d0 ,
252   den_min = 1.d-12,
253   if_unneutralized = .true.,
254   num_dgam = 1,
255   dgam = 479.6,
256   n_sort = 0,
257  }
258
259
260  !-------------- density profile for species 3--------------------
261  !actual profile data
262
263  num_x
264  {
265  num_x = 6,
266  }
267
268  profile
269  {
270  profile_type(1:2) = gaussian, piecewise-linear,
271  f_cent(1) = 0.001,
272  x_cent(1) = 100.0,
273  x_sigm(1) = 0.0785,
274  n_sigm(1) = 3,
275  fx(1:6,2) = 1, 1, 1, 1, 1, 1,
276  x(1:6,2) = 0, 0.9, 1.0, 1.0, 1.0, 3.0,
277  }
278
279
280  !-------------- boundary conditions for species 3-----------------
281
282  spe_bound
```

```
283  {
284   type(1,1) = 5, type(2,1) = 5,
285   type(1,2) = 5, type(2,2) = 5,
286  }
287
288
289  !-------------- diagnostic for species 3 -------------------
290
291  diag_species
292  {
293  ndump_fac_pha = 1,
294  ps_xmin(1:2) = 0, 0,            ps_pmin(1:3) = 0, -5, -5,
295  ps_xmax(1:2) = 150.0, 3.0,      ps_pmax(1:3) = 500, 5, 5,
296  ps_nx(1:2) = 1500.0, 3.0,       ps_np(1:3) = 250, 200, 200,
297   if_x2x1 = .true. ,
298   if_p1x1 = .true. ,
299   if_p2x1 = .true. ,
300   if_p3x1 = .false. ,
301   if_p1x2 = .true. ,
302   if_p2x2 = .true. ,
303   if_p3x2 = .false. ,
304   if_p2p1 = .true. ,
305   if_p3p1 = .false.,
306   if_p3p2 = .false.,
307  }
308
309
310
311  !-------------- number of pulses ---------------------------
312
313  pulse_sequence
314  {
315   num_pulses = 0,
316  }
317
318  !--------------------- information for pulse 1 -------------------
319
320  pulse
```

```
{
 iflaunch = .false., wavetype = 1,
 w0 = 100, rise = 90, fall = 90, length = 0.00,
vosc = .6, rkkp = 1, pol = 90, phase = 0,
start = 0, focus = -300, offset(1) = 0,
 time = 0.0,
}
!--------------------- information for pulse 2 ------------------
pulse
{
 iflaunch = .false. , wavetype = 1,
 w0 = 20, rise = 90, fall = 90, length = 0.00,
vosc = 1.5, rkkp = 1, pol = 90, phase = 0,
start = 180, focus = -300, offset(1) = 0,
 time = 0.0,
}


smooth
{
 ifsmooth(1) = .false.,
 smooth_level(1) = 3,
 swfj(1,1,1) = 1, swfj(2,1,1) = 2, swfj(3,1,1) = 1,
 swfj(1,2,1) = 1, swfj(2,2,1) = 2, swfj(3,2,1) = 1,
 swfj(1,3,1) = 1, swfj(2,3,1) = 2, swfj(3,3,1) = 1,
 ifsmooth(2) = .false.,
 smooth_level(2) = 3,
 swfj(1,1,2) = 1, swfj(2,1,2) = 2, swfj(3,1,2) = 1,
 swfj(1,2,2) = 1, swfj(2,2,2) = 2, swfj(3,2,2) = 1,
 swfj(1,3,2) = 1, swfj(2,3,2) = 2, swfj(3,3,2) = 1,
}

!--------------- diagnostic for currents --------------------------

diag_phy_field
{
 ndump_fac_all = 1, file_name_all = ' ',
 ndump_fac_ave = 0, file_name_ave = ' ',
```

```
359    n_ave(1:2) = 2, 2,
360    ifdmp_phy_field(1:3) = .true. , .true. , .false. ,
361   }
362
363
364   !----------------- smoothing for charge ----------------------
365
366   smooth
367   {
368    ifsmooth(1) = .false.,
369    smooth_level(1) = 3,
370    swfj(1,1,1) = 1, swfj(2,1,1) = 2, swfj(3,1,1) = 1,
371    swfj(1,2,1) = 1, swfj(2,2,1) = 2, swfj(3,2,1) = 1,
372    swfj(1,3,1) = 1, swfj(2,3,1) = 2, swfj(3,3,1) = 1,
373    ifsmooth(2) = .false.,
374    smooth_level(2) = 3,
375    swfj(1,1,2) = 1, swfj(2,1,2) = 2, swfj(3,1,2) = 1,
376    swfj(1,2,2) = 1, swfj(2,2,2) = 2, swfj(3,2,2) = 1,
377    swfj(1,3,2) = 1, swfj(2,3,2) = 2, swfj(3,3,2) = 1,
378   }
379
380   !---------------- diagnostic for charge --------------------
381
382   diag_phy_field
383   {
384    ndump_fac_all = 0, file_name_all = ' ',
385    ndump_fac_ave = 0, file_name_ave = ' ',
386    n_ave(1:2) = 2, 2,
387    ifdmp_phy_field(1) = .true.,
388   }
389
390   !--------------- antenna parameters ------------------
391
392   antenna_array
393   {
394    n_antenna = 0,
395   }
396
```

```
antenna
{
 a0 = 0.50, omega0 = 1.0,
t_rise = 753.5, t_fall = 753.5, t_flat = 0.00,
w0 = 44.0,  w0_2= 44.0,
x0 = 157.1,
ant_type = 1, delay = 0,
spin = 0, phase = 0, pol=0, tilt=0,  focus = 251.33,
}

antenna
{
 a0 = 0.50, omega0 = 1.0,
t_rise = 753.5, t_fall = 753.5, t_flat = 0.00,
w0 = 44.0,  w0_2= 44.0,
x0 = 157.1,
ant_type = 1, delay = 90,
spin = 0, phase = 0, pol=90, tilt=0,  focus = 251.33,
}
```